Association of SPIN90, Arp2/3 complex, and formin mDia1 controls cortical actin organization

Luyan Cao[1]*, Amina Yonis[2,3]*, Malti Vaghela[2,4]*, Elias H Barriga[3,12], Priyamvada Chugh[5], Matt Smith[5,13], Julien Maufront[6,7], Geneviève Lavoie[8], Antoine Méant[8], Emma Ferber[2], Miia Bovellan[2,3], Art Alberts[9,†], Aurélie Bertin[6,7], Roberto Mayor[3], Ewa K. Paluch[5,10,14], Philippe P. Roux[8,11], Antoine Jégou[1,#], Guillaume Romet-Lemonne[1,#], Guillaume Charras[2,3,10,#]

Supplementary information

Supplementary figures

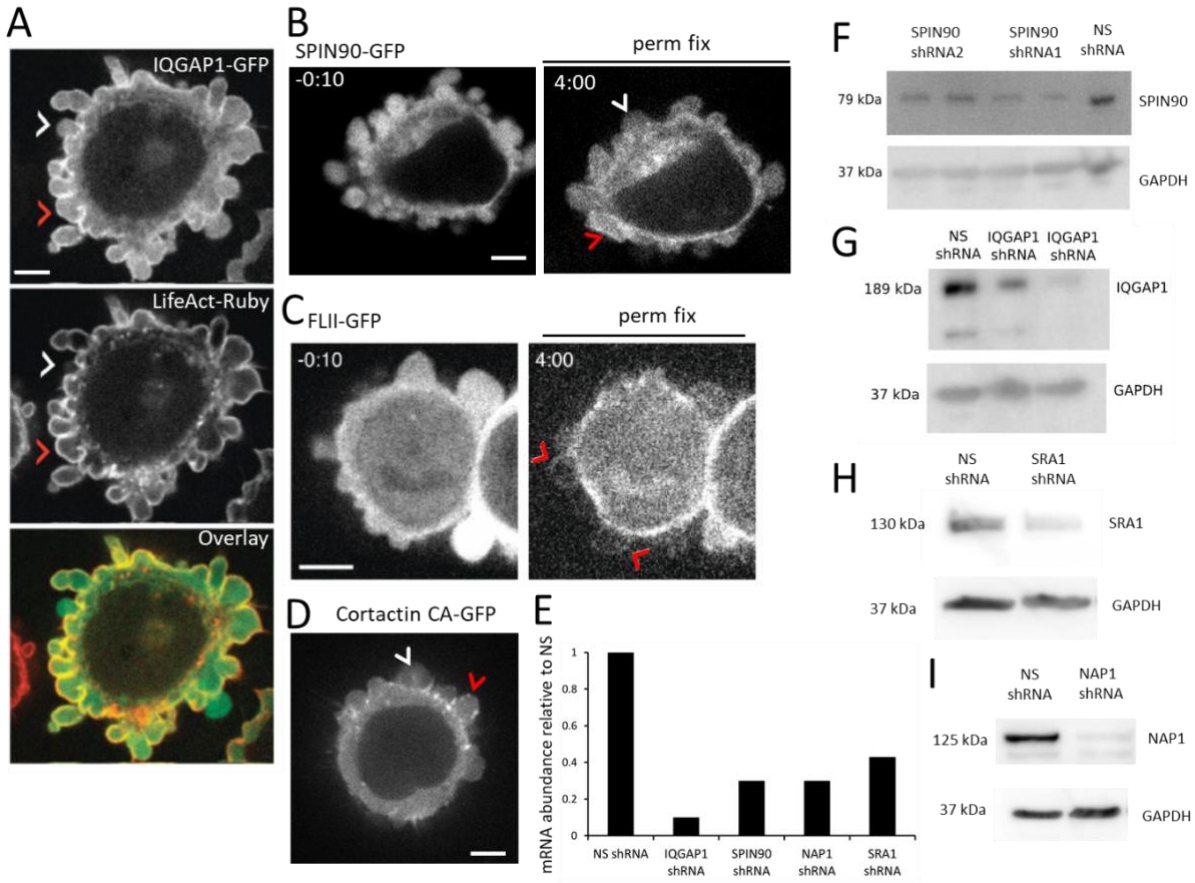

Supplementary Fig S1 related to Figure 1. A. Confocal microscopy image of a blebbing M2 melanoma cell expressing IQGAP1-GFP and LifeAct-Ruby. IQGAP1 localizes to the rim of retracting blebs (red arrowhead) but not to the rim of nascent blebs (white arrowhead). **B.** Confocal microscopy images of a blebbing M2 melanoma cell expressing SPIN90-GFP before (left) and after (right) permeabilization and fixation. Following permeabilization and fixation, SPIN90 remains localized to the actin cortex of retracting blebs (red arrowhead) but is absent from the cortex of nascent blebs (white arrowhead). **C.** Confocal microscopy images of a blebbing M2 melanoma cell expressing FLII-GFP before (left) and after (right) permeabilization and fixation. Following permeabilization and fixation, FLII remains localized to the actin cortex of retracting blebs, red arrowheads. **D.** Confocal microscopy image of a blebbing melanoma cell expressing constitutively active cortactin-GFP. Active cortactin localizes to the rim of retracting blebs (red arrowhead) but not to the rim of nascent blebs (white arrowhead). (**A-D**) White arrowheads indicate expanding blebs and red arrowheads retracting ones. Scale bars=5µm. **E.** mRNA abundance in M2 cells stably expressing shRNA constructs targeting IQGAP1, SPIN90, NAP1, SRA1, and Non-silencing shRNA (NS shRNA). The graph shows mRNA expression levels relative to control non-silencing shRNA construct for each target. Abundance was normalized to GAPDH mRNA levels. Differences were considered significant if relative mRNA abundance was reduced by at least 40%. Data is averaged over two independent experiments. **F.** Immunoblot of M2 cells stably transfected with non-silencing shRNA, SPIN90 shRNA1, SPIN90 shRNA2 and probed with anti-SPIN90 and anti-GAPDH. **G.** Immunoblot of M2 cells stably transfected with non-silencing shRNA and IQGAP1 shRNA and probed with anti-IQGAP1 and anti-GAPDH. **H**. Immunoblot of M2 cells stably transfected with non-silencing shRNA and SRA1 shRNA and probed with anti-SRA1 and anti-GAPDH. **I**. Immunoblot

of M2 cells stably transfected with non-silencing shRNA and NAP1 shRNA and probed with anti-Nap1 and anti-GAPDH.

Assay\Depletion	Arp2/3	WRC	mDia1	IQGAP1	SPIN90
Blebbing index (M2, **Fig 1G**)	0.5 [2]	0.2	1.9 [2]	1.4	1.3
Cell death(HeLa, **Fig 1H-I**)	1.3	1.1	3.6	2.1	3.0
Mesh, % large gaps (M2, **Fig 2A-B**)	0.6	2.3	6.0	2.1	0.7
Mesh, % small gaps (M2, **Fig 2A-B**)	1.1	0.9	1.1	1.1	1.2
Cortical density (HeLa, **Fig 2E**)	1.0	1.2	1.1	0.9	1.5
Cortical thickness (HeLa, **Fig 2D**)	0.9 [1]	0.8	0.8 [1]	1.0	0.8
Cortical pMLC (HeLa, **Fig S6B**)	0.8 [1]	0.9	1.0 [1]	1.0	1.0
Actin accumulation rate (HeLa, **Fig 2H-I**)	1.8	1.3	0.7	0.7	0.8
Cortical stiffness (HeLa, **Fig 2K-L**)	2.0	2.7	1.1	0.9	2.0

[1] Data from Chugh et al, Nature Cell Biology, 2017
[2] Data from Bovellan et al, Current Biology, 2014

Fig S2 related to Figures 1-2. Graphic summary of experimental findings in cellular assays. The depletion target is indicated in the top row. The left hand side column indicates the assay considered, the cell type it was performed in, and the figure panel it relates to. All data is normalized to the value for the appropriate control. Each cell is color coded with blue indicating statistically significant decreases relative to control and red indicating statistically significant increases relative to control. [1] Data from Chugh et al[1]. [2] Data from Bovellan et al[2].

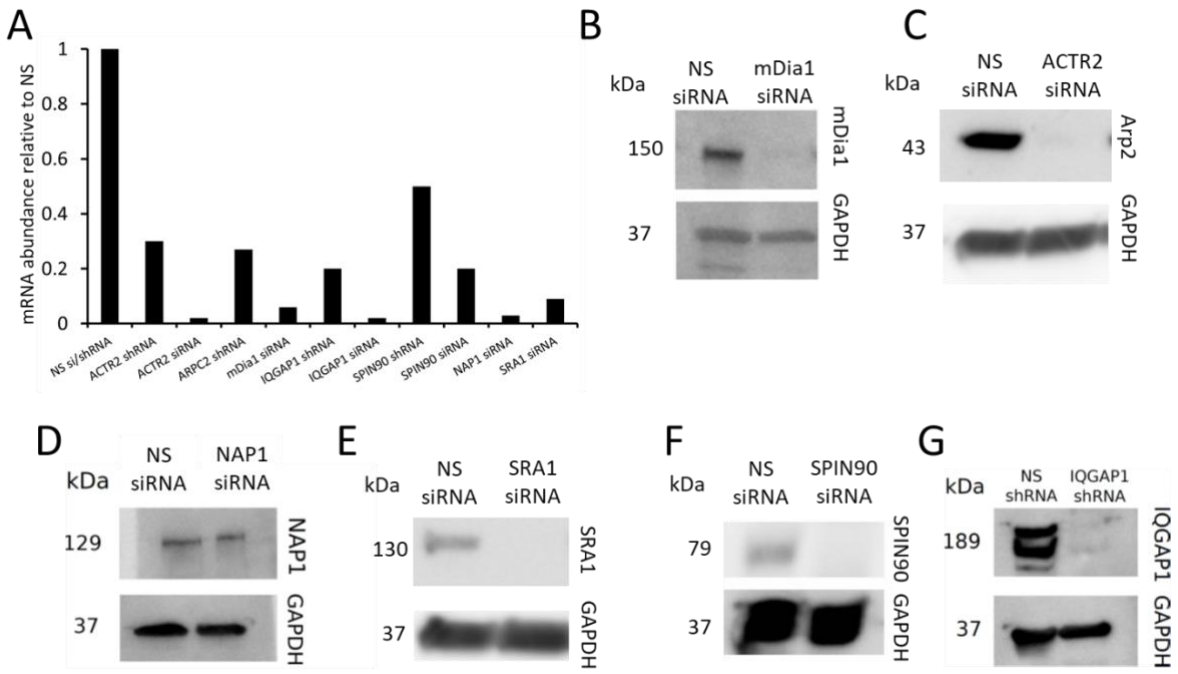

Figure S3 related to Figure 1. A. mRNA abundance in HeLa cells stably expressing shRNA constructs or transiently transfected with siRNA. Targets and the nature of silencing are indicated on the x-axis. The graph shows mRNA expression levels relative to control non-silencing sh/siRNA (NS si/shRNA) construct for each target. Abundance was normalized to GAPDH mRNA levels. Differences were considered significant if relative mRNA abundance was reduced by at least 40%. Data is averaged over two independent experiments. **B.** Immunoblot of HeLa cells transiently transfected with non-silencing siRNA or mDia1 siRNA and probed with anti-mDia1 and anti-GAPDH. **C.** Immunoblot of HeLa cells transiently transfected with non-silencing siRNA or ACTR2 (the Arp2 subunit of the Arp2/3 complex) siRNA and probed with anti-Arp2 and anti-GAPDH. **D.** Immunoblot of HeLa cells transiently transfected with non-silencing siRNA or NAP1 siRNA and probed with anti-NAP1 and anti-GAPDH. **E.** Immunoblot of HeLa cells transiently transfected with non-silencing siRNA or SRA1 siRNA and probed with anti-SRA1 and anti-GAPDH. **F.** Immunoblot of HeLa cells transiently transfected with non-silencing siRNA or SPIN90 siRNA and probed with anti-SPIN90 and anti-GAPDH. **G.** Immunoblot of HeLa cells stably transfected with non-silencing shRNA or IQGAP1 shRNA and probed with anti-IQGAP1 and anti-GAPDH.

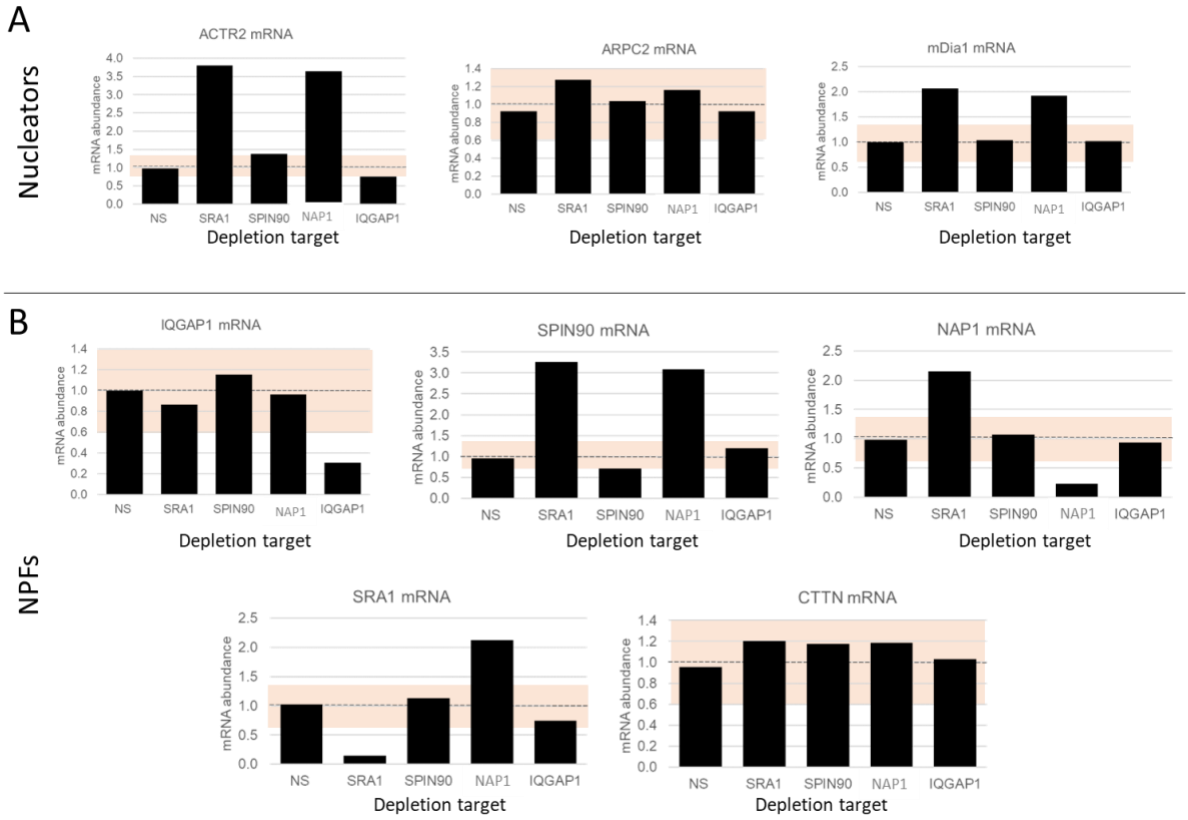

Figure S4 related to Figure 1. mRNA abundance in HeLa cells stably transfected with shRNA constructs. Each graph shows the abundance of one mRNA transcript for depletion of the targets shown on the x-axis. mRNA expression levels are computed relative to non-silencing shRNA (NS). Abundance was normalized to GAPDH and ACTB mRNA levels. Differences were considered significant if relative mRNA abundance was increased or reduced by at least 40%. Shaded red regions show mRNA abundances not significantly different from NS control. Data is averaged over two independent experiments. **A.** changes in nucleator transcript mRNA in response to depletion of NPFs. **B.** Changes in NPF transcript mRNA in response to depletion of NPFs. Only depletion of SRA1 and NAP1 lead to significant changes in nucleator or NPF abundances.

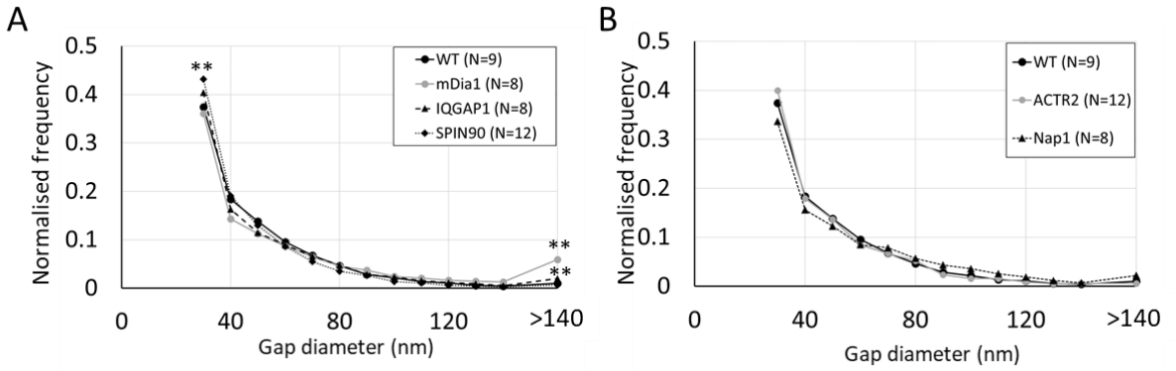

Figure S5 related to Figure 2A-B. Frequency distribution of gap diameters within the cortical mesh of blebs in M2 cells. **A.** Gap size distribution for WT cells and cells depleted in mDia1, IQGAP1, and SPIN90. **B.** Gap size distribution for WT cells and cells depleted in ACTR2, NAP1. (**A-B**) Data points showing a significant change in proportion compared to WT are indicated by asterisks (**p≤0.01). Comparison to WT with Wilcoxon's rank test for small mesh sizes (<30nm): Arp2: p=0.03; Nap1: p=0.12; mDia1: p=0.08; IQGAP1: p=0.04; SPIN90: p=0.01. For large mesh sizes (>140nm): Arp2: p=0.24; Nap1: p=0.09; mDia1: p=0.01; IQGAP1: p=0.01; SPIN90: p=0.81.

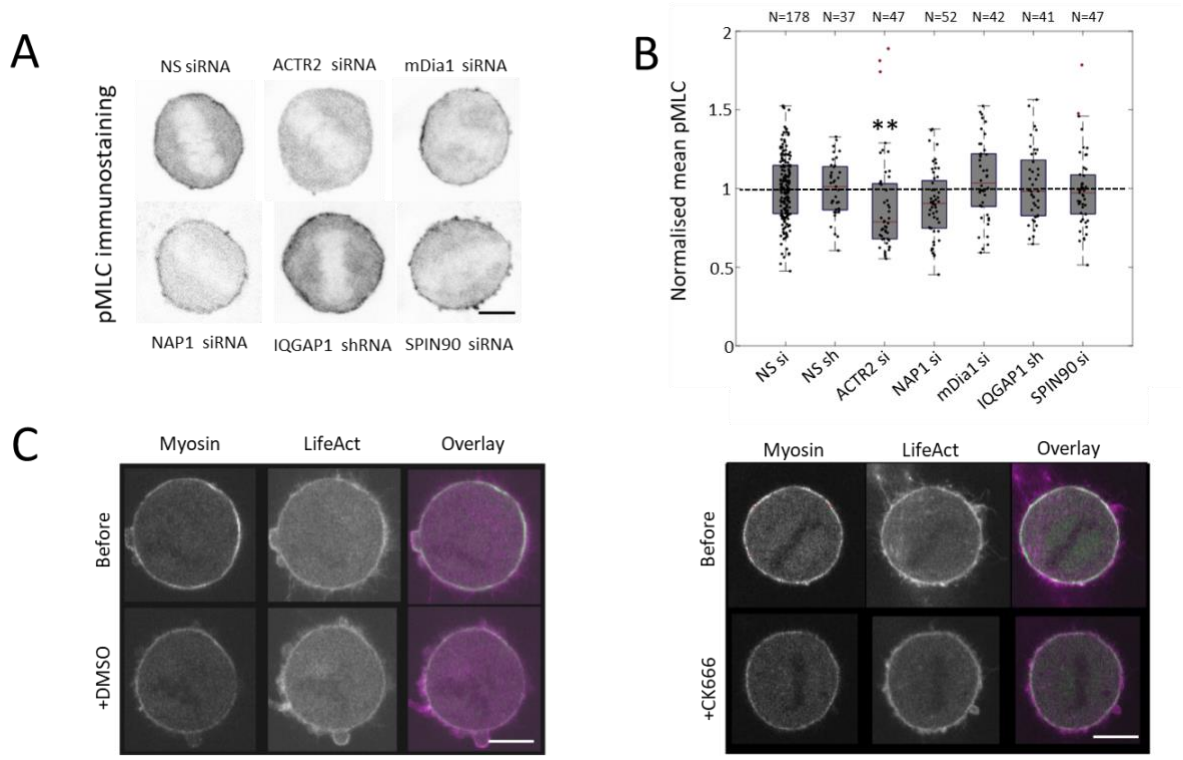

Figure S6 related to Figure 2. A. Representative pMLC distribution in metaphase HeLa cells visualized by immuno-staining for different protein depletions and for non-silencing (NS) siRNA. Each image is a single section of a confocal microscopy stack and is shown in inverted contrast. **B.** Mean cortical pMLC fluorescence intensity for different treatments normalized to the mean cortical pMLC fluorescence intensity for non-silencing (NS) siRNA or shRNA. Data are plotted as box-whisker plots. Whiskers indicate minimum and maximum values. The number of cells examined is indicated above the boxplot. Statistical outliers are indicated by a red dot. **$p < 0.01$ compared to the appropriate control. See **Fig S16** for controls. **C.** Change in cortical myosin regulatory light chain fluorescence intensity upon treatment with DMSO (left panel) or CK666 (right panel). In each panel, the top row shows the fluorescence intensity before treatment and the bottom row after treatment for the same cell. The left most column shows myosin regulatory light chain fluorescence (MRLC-GFP), the middle column shows LifeAct-Ruby, and the right column shows the overlay with MRLC in green and LifeAct in Magenta. (**A,C**) Scale bars=10µm.

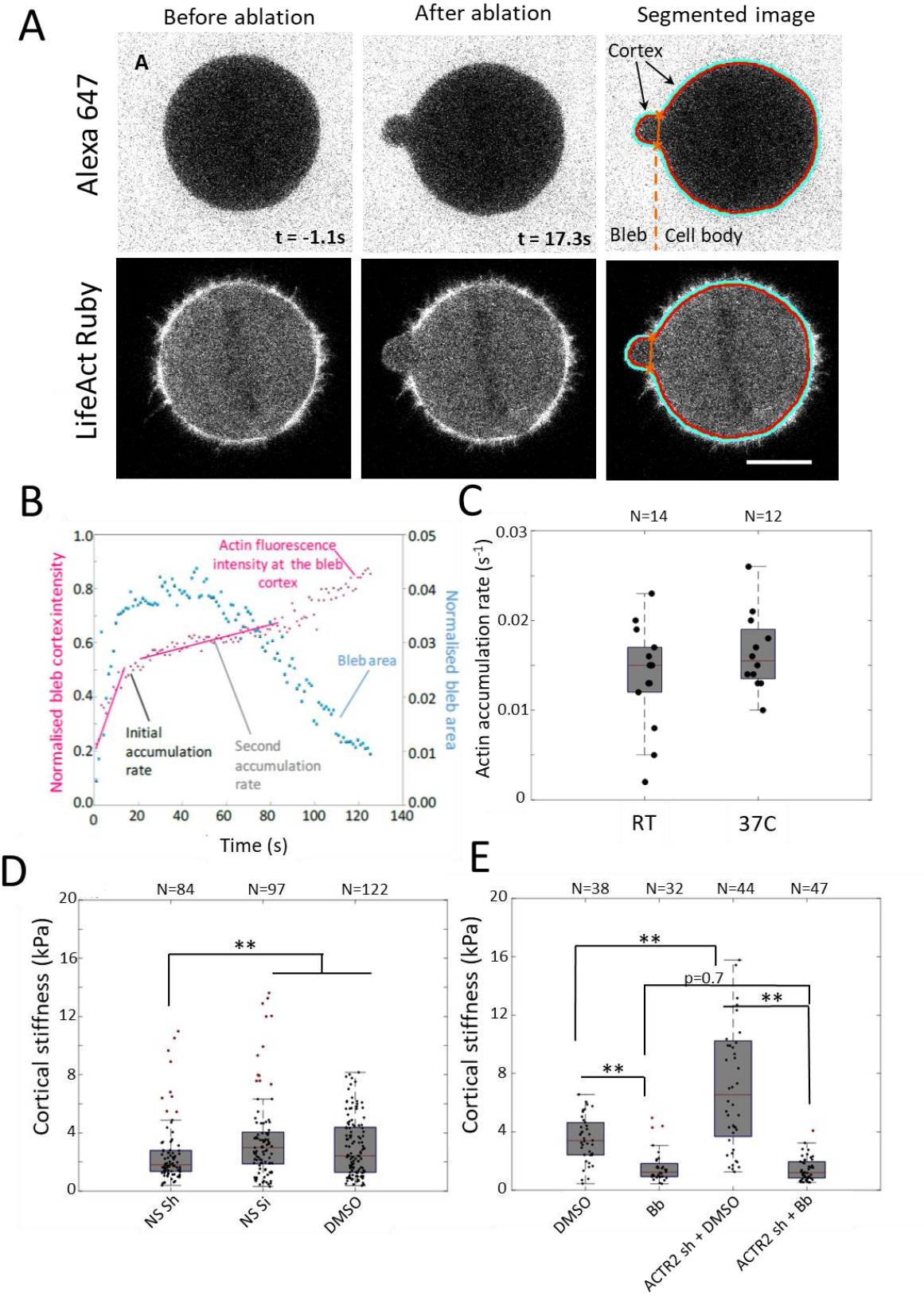

Figure S7 related to Figure 2. A. Representative laser ablation experiment. All images are one optical section of a confocal microscopy stack. Top row shows Alexa647 fluorescence. Alexa647 is added to the medium to allow for robust segmentation of the cell from the medium using dye exclusion. Bottom row shows LifeAct Ruby fluorescence, a reporter for F-actin. The left hand column shows the cell

before ablation. The middle column shows the cell after ablation. The right hand column shows the segmentation. Timings are indicated in the bottom right corner of the top row. Scale bar 10µm. **B.** Representative actin regrowth curve as a function of time in a bleb induced by laser ablation in a metaphase HeLa cell expressing LifeAct-Ruby. The mean actin fluorescence intensity at the bleb cortex was normalized to the mean intensity in the cell body cortex (pink). The temporal evolution of bleb area normalized to the cell body area is plotted in blue. Initial regrowth rates after ablation are linear with time (initial accumulation rate). t = 0 s, ablation onset. **C**. Actin accumulation rate determined in metaphase cells at 37C and at Room Temperature are not significantly different. **D.** Apparent elastic modulus for cells expressing Non-Silencing shRNA (NS sh), Non-Silencing siRNA (NS si), and treated with DMSO. **E.** Apparent elastic modulus of WT cells treated with DMSO and blebbistatin compared to cells depleted in ACTR2 treated with DMSO and blebbistatin. WT cells treated with DMSO have a significantly lower apparent elasticity than cells expressing shRNA targeting ACTR2 and treated with DMSO. WT cells treated with blebbistatin do not have a significantly different apparent elasticity compared to ACTR2 depleted cells treated with blebbistatin. This suggests than the increase in apparent elastic modulus observed in ACTR2 depleted cells is due to an increase in cortical tension mediated by myosin. **(C-E)** Data are plotted as box-whisker plots. Whiskers indicate minimum and maximum values. The number of measurements is indicated above each box. Statistical outliers are indicated by a red dot. **$p < 0.01$ compared to the appropriate control.

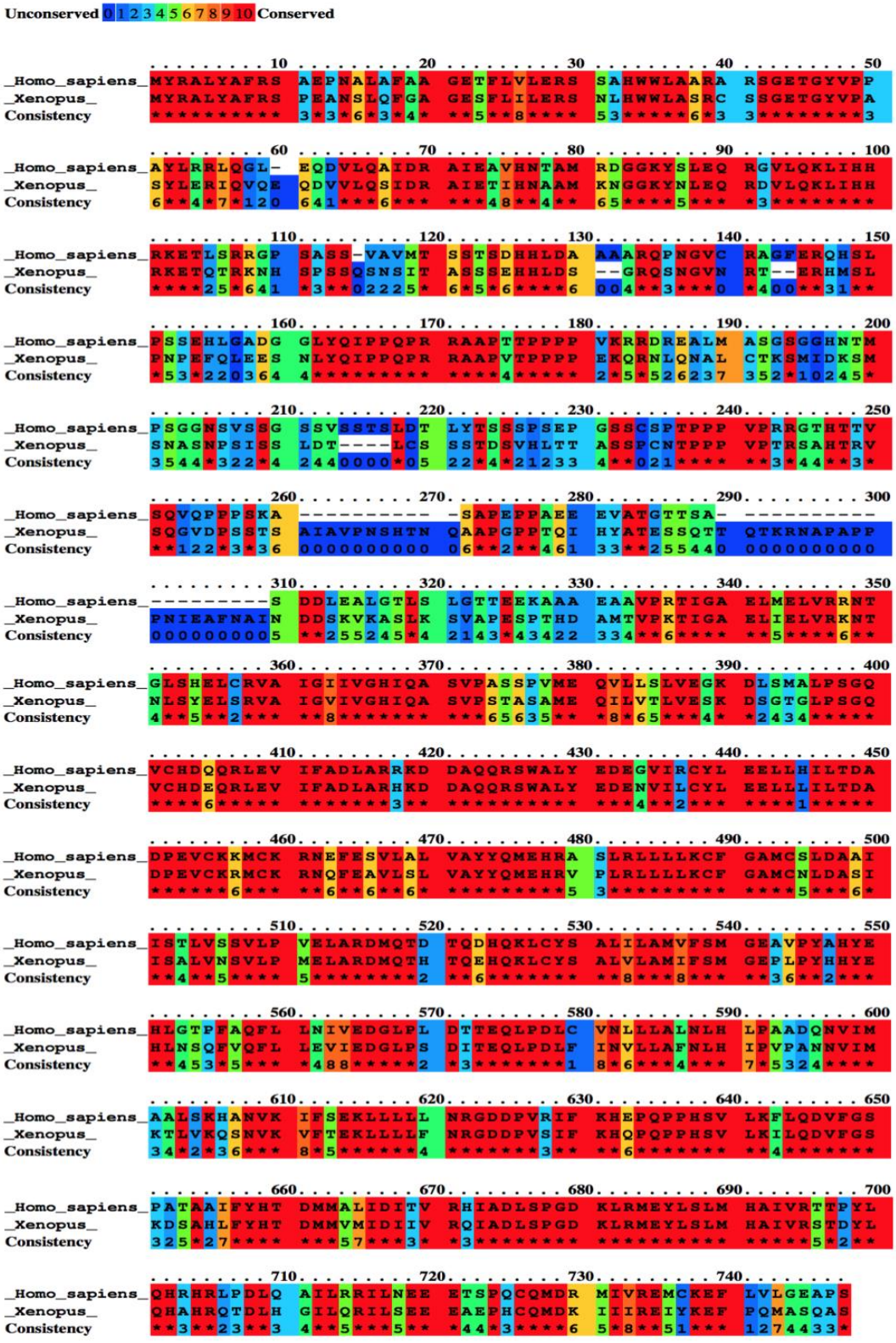

Supplementary Fig S8 related to Figure 3. Alignment of human SPIN90 and *Xenopus Laevis* SPIN90. Conserved regions appear in red and divergent regions appear in blue. High homology is present in the N and C terminuses of the protein.

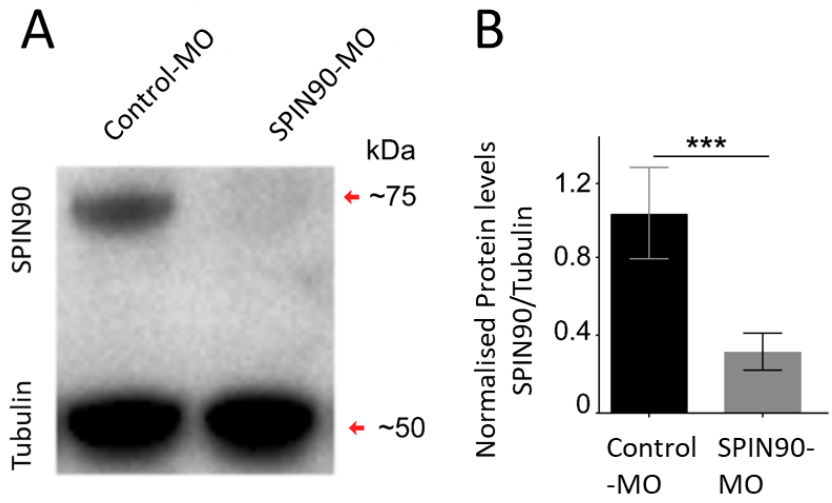

Supplementary Fig S9 related to Figure 3.

A. Immunoblot of *Xenopus* embryos microinjected with Control-MO or SPIN90-MO. The blot is probed with anti-SPIN90 and anti-tubulin. **B.** Graph showing SPIN90 protein levels normalized to the house keeping marker α-tubulin. Bars represent mean ± S.E two tailed *t*-test p***<0.001. Results from 4 independent experiments.

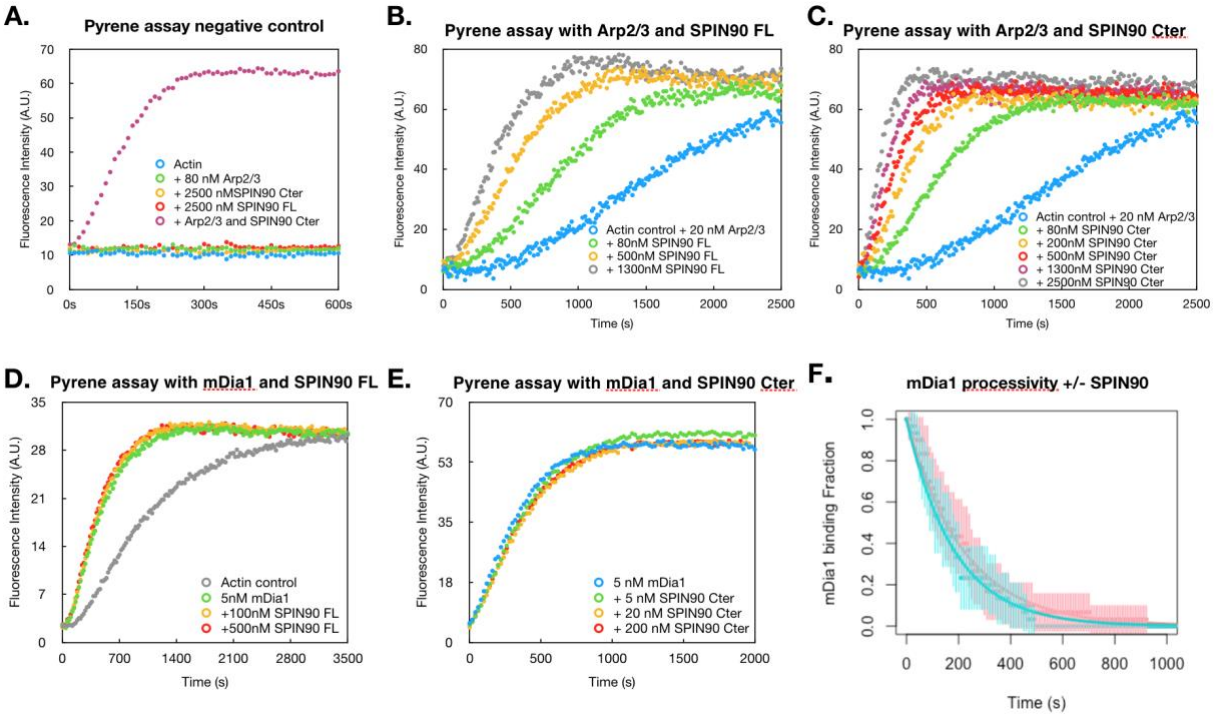

Fig S10 related to Figure 4: Characterization of the interaction of SPIN90 with mDia1 and Arp2/3. (**A-E**)**.** Actin assembly was detected by the change in pyrenyl-actin fluorescence in a Safas Xenius spectrofluorimeter (Safas) at room temperature. **A.** Pyrene-actin polymerization assay (2 µM actin) shows that the presence of Arp2/3 or SPIN90 alone does not accelerate actin polymerization but that, when both are included, actin polymerization is accelerated (pink curve). **B.** Pyrene-actin polymerization assay with 2.5 µM actin, 20 nM Arp2/3 and various concentrations of full-length SPIN90. **C.** Pyrene-actin polymerization assay with 2.5 µM actin, 20 nM Arp2/3 and various concentrations of the C-terminal portion of SPIN90 (aa 269-722). **D.** Pyrene-actin polymerization assay with 2.5 µM actin, 5 nM mDia1 and various concentrations of full-length SPIN90. **E.** Pyrene-actin polymerization assay with 5 nM mDia1 and various concentrations of the C-terminal portion of SPIN90. **F.** Processivity of mDia1 with and without SPIN90. In a microfluidics setup, filaments were rapidly elongated by mDia1 at their barbed ends, with their pointed ends anchored to the surface by spectrin-actin seeds. The presence of mDia1 at the barbed end was indicated by the rapid elongation of the filaments[3]. The plot shows the fraction of mDia1-bound barbed ends as a function of time. The filaments are exposed to 0.5µM actin and 3.5µM profilin with (blue points) or without (red points) 0.1µM full-length SPIN90. The results indicate that SPIN90 does not have a measurable impact on mDia1's processivity (p=0.4, log-rank test). Solid lines indicate exponential fits and shaded regions indicate 95% confidence intervals.

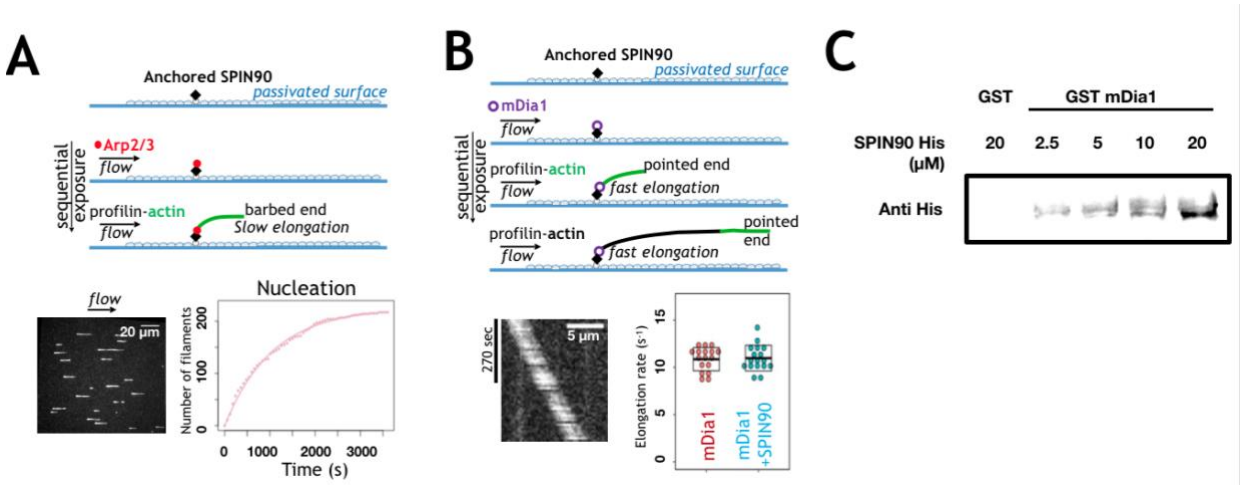

Fig S11 related to Figure 4: Characterization of the interaction of SPIN90 with mDia1 and Arp2/3.

A. Sketch of a microfluidics experiment, where surface-anchored SPIN90 is exposed to 30nM Arp2/3 complex for 5 min, followed by profilin-actin (15% Alexa488 labeled). TIRF microscope image: filaments nucleate and grow from their free barbed ends while their pointed ends remain attached. Plot: appearance of 217 filaments over time (red dots), with an estimated nucleation rate of 9.5×10^{-4} s^{-1} (exponential fit, solid line). **B.** Microfluidics experiment where surface-anchored SPIN90 is exposed to 50nM mDia1 for 5 min, followed by profilin-actin (15% Alexa488 labeled) and then profilin-actin (unlabeled). Kymograph (from TIRF microscopy): filaments grow rapidly from their anchored barbed ends. Plot: elongation rate of these filaments (blue, n=17) compared to filaments growing from mDia1 directly anchored to the surface without SPIN90 (red, n=17). Boxes indicate averages and standard deviation. **C**. GST pull down assay to detect binding between mDia1 and SPIN90. GST or GST-fused mDia1 coated beads were incubated with various concentrations of His tag-fused SPIN90 for 1 hour. Proteins attached to the beads were eluted with 20 mM GSH. The presence of SPIN90 was detected by western blot. The experiments were repeated three times.

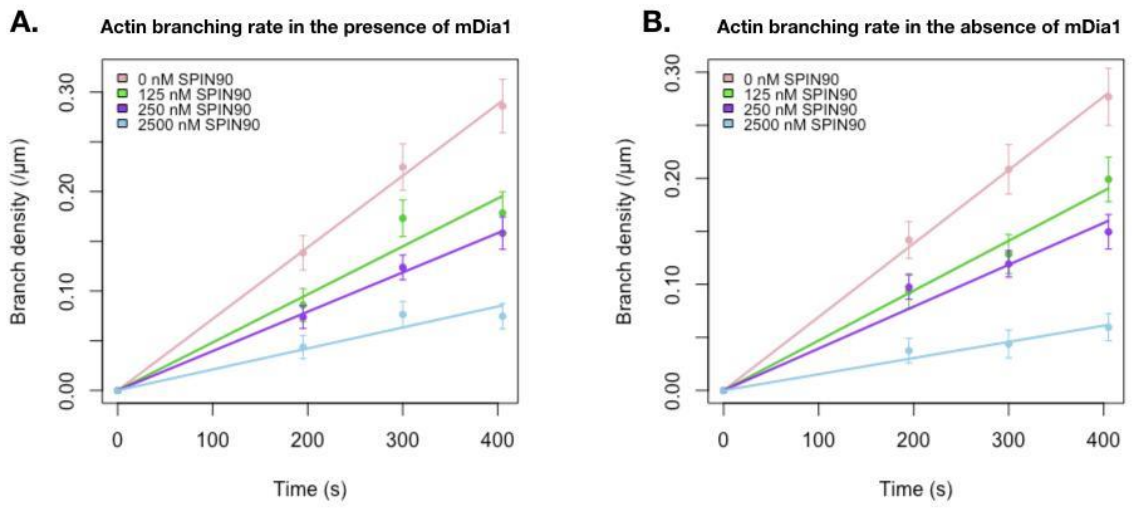

Fig S12 related to Fig 4D. Preformed actin filaments labelled with 15% Alexa568 were mixed with 0.5µM G-actin (15% Alexa488 labelled), 0.5µM profilin, 20nM Arp2/3 complex, 50nM VCA along with various concentrations of SPIN90 and with (panel **A**) or without (panel **B**) 0.2nM mDia1. For each SPIN90 concentration, the branch density on the preformed mother filaments as a function of time was fitted with a linear function. Its slope represents the branching rate. The resulting branching rates are plotted in **Fig. 4D**.

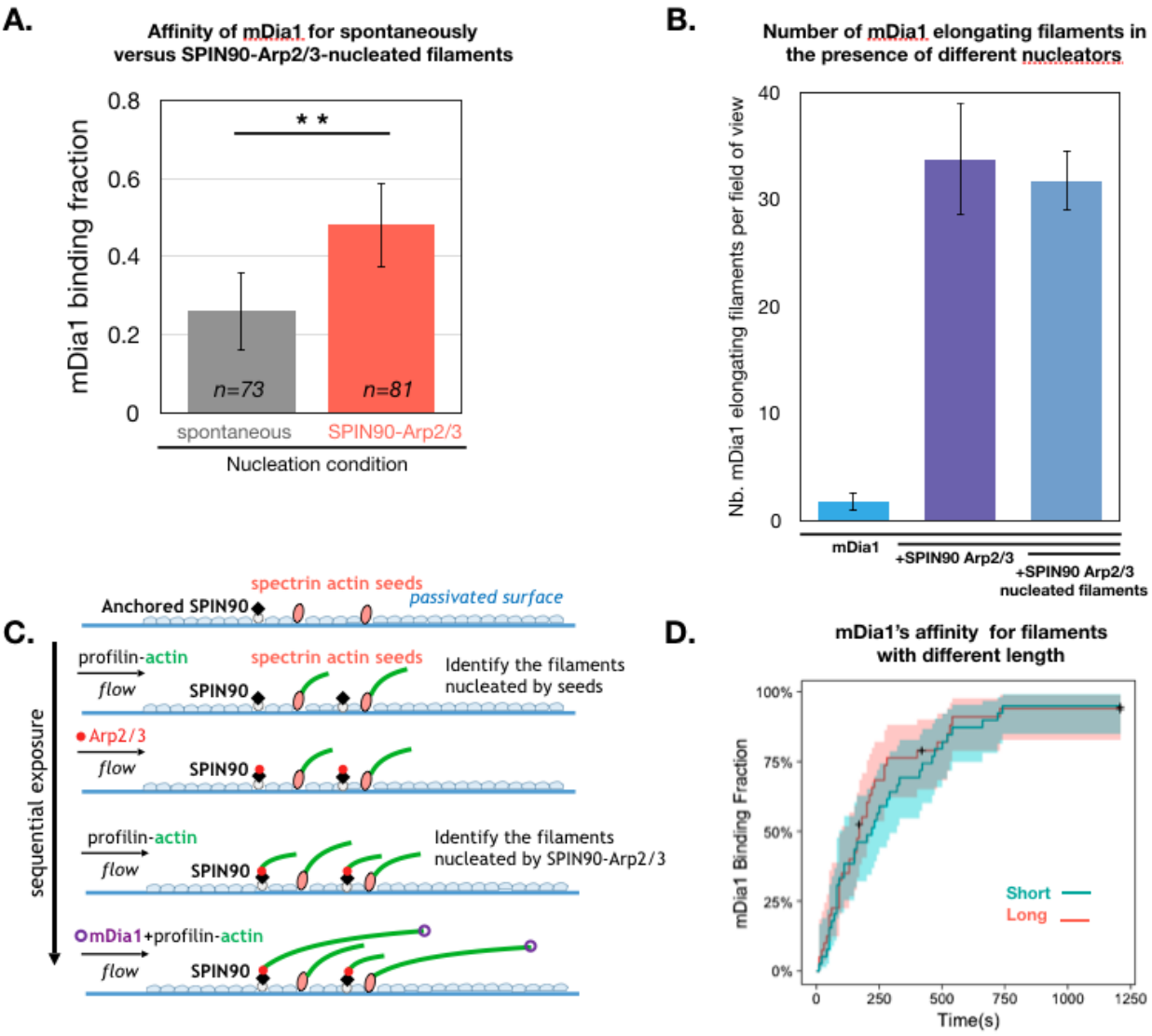

Fig S13 related to Fig 5. A. Comparison of the affinity of mDia1 for spontaneously nucleated versus SPIN90-Arp2/3-nucleated filaments (related to **Fig. 5B**, here with inverted fluorophores). Spontaneously nucleated actin filaments (formed with 15% Alexa488 labelled G-actin) were mixed with SPIN90-Arp2/3-nucleated actin filaments (formed with 15% Alexa568 G-actin) along with 0.2nM mDia1, 0.5 µM profilin and 0.5 µM G-actin (containing 3% Alexa488 labelled G-actin). The bar chart represents the fraction of rapidly growing barbed ends within each population, observed after 300 seconds. Comparison with a Pearson's chi square test: p=0.007. **B.** Number of filaments elongated by mDia1 (identified by their rapid elongation) per field of view, after 10 minutes, in the presence of 0.5 µM G-actin (15% Alexa488 labelled), 0.6 µM profilin, and 0.2 nM mDia1 supplemented with, from left to right: 1) nothing; 2) 250 nM SPIN90 and 25 nM Arp2/3; 3) 250 nM SPIN90 and 25 nM Arp2/3 and filaments preformed with 250 nM SPIN90 and 25 nM Arp2/3 and actin (Alexa568 labeled) which are excluded from the count. The results indicate that, in these conditions, the nucleation of filaments by mDia1 alone is negligible compared to nucleation by SPIN90-Arp2/3 (comparing 1 and 2), and that the potential contribution of short preformed filaments which could be misinterpreted as newly nucleated during the experiment is negligible (comparing 2 and 3). **C.** Sketch of microfluidics experiment related to **Fig 5C**, showing how two groups of filaments generated by different nucleators were generated and identified. SPIN90 and spectrin-actin seeds were anchored to the surface (first row), and were first exposed to 0.7 µM 15% Alexa488 G-actin to generate filaments nucleated from the seeds (second

row). Then Arp2/3 was flowed in (3rd row), followed by 0.7 µM 15% Alexa488 G-actin to generate SPIN90-Arp2/3 nucleated filaments (4th row). Since all the spectrin-actin seeds had already nucleated filaments during the first exposure to actin, the newly nucleated filaments were identified as being nucleated by SPIN90-Arp2/3. Finally, mDia1 was introduced into the chamber with profilin-actin (5th row). **D**. mDia1's affinity for filaments with different lengths, related to **Fig. 5B** and **5C**. To check whether mDia1 had a different affinity for filaments with different lengths, filaments nucleated by spectrin-actin seeds in a microfluidics setup, with heterogeneous lengths, were exposed to 0.4 nM mDia1, 0.5 µM 15% Alexa488 G-actin and 3.5 µM profilin. The binding affinity of mDia1 for long filaments nucleated by spectrin actin seeds (>5 µm, N=40) was compared to that for short filaments nucleated by spectrin actin seeds (<1 µm, N=39). Our results indicate that the length of the filaments does not have an effect on mDia1's binding efficiency (p=0.6, log-rank test).

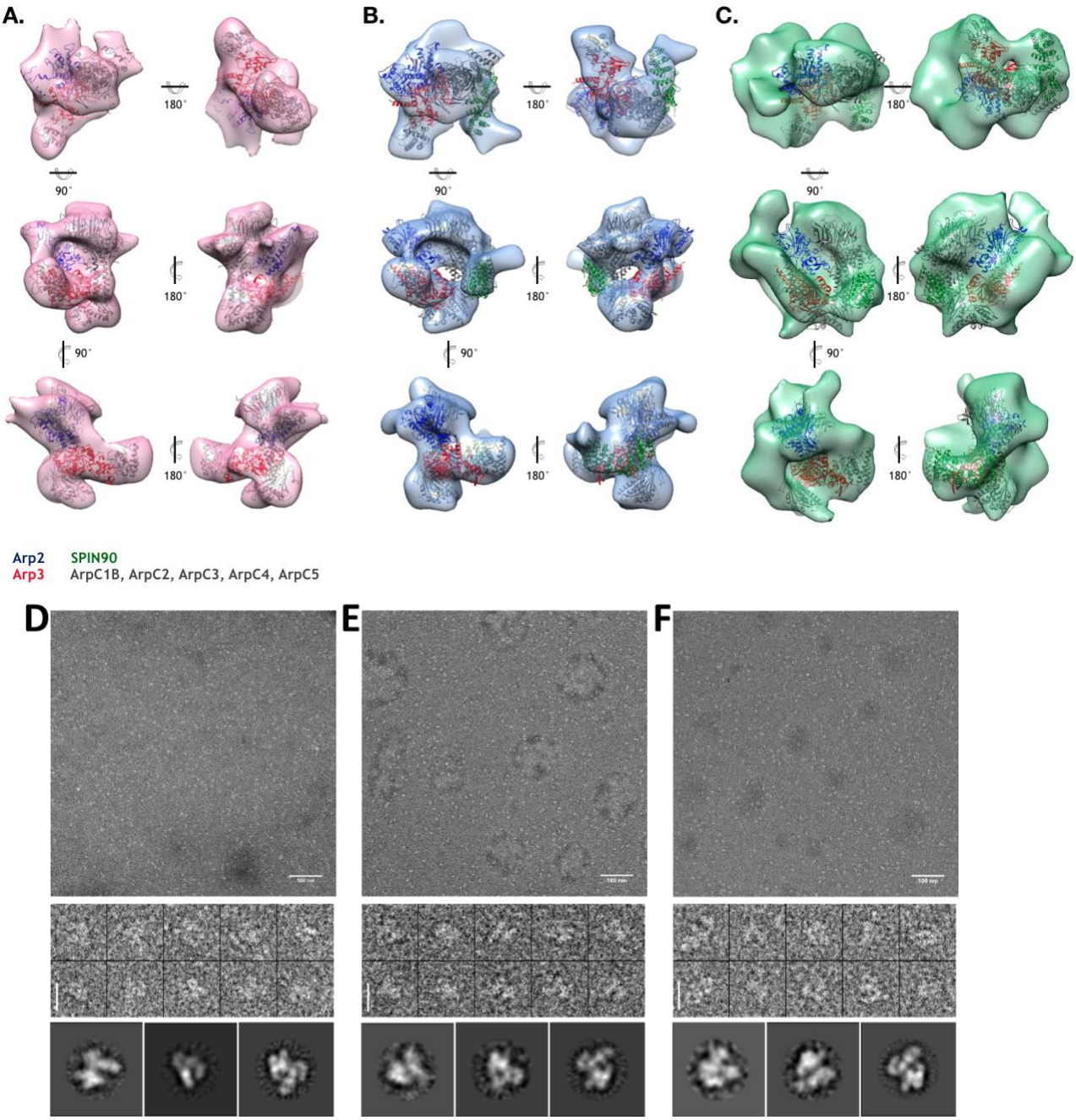

Fig S14 related to Figure 6B: Different combinations of complexes (binary or ternary) involving the Arp2/3 complex, SPIN90, and mDia1 were analyzed by electron microscopy and single particle analysis. For each protein complex, three-dimensional reconstructions were obtained from 3D classifications and compared to existing or generated crystal structures (see methods). **A.** Incubation of mDia1 and Arp2/3 resulted in a 3D structure which only accommodates Arp2/3, suggesting that mDia1 and Arp2/3 do not interact when SPIN90 is absent. **B.** Conversely, mixing the Arp2/3 complex and SPIN90 results in a complex for 76 % of the particles. Within the complex, SPIN90 (green) clearly appears as an additional density when compared with the truncated docked crystal structure. **C.** When compared with the Arp2/3-SPIN90 complex in B, the 3D envelope (resolution of 27 Å) resulting from the ternary complex (SPIN90-Arp2/3-mDia1) exhibits an additional density accommodating a dimer of FH2 domains for 22 % of the particles. **D-F.** Raw data of Arp2/3, SPIN90, mDia1 negatively stained (scale bars: 100 nm in upper images, 15 nm in middle images; lower boxes are 29.8 nm^2). **D.** Micrograph of Arp2/3 mixed with mDia1 (top), subselection of particles used for Arp2/3 3D reconstruction (middle), and examples of 2D classes (bottom). **E.** Micrograph of Arp2/3 mixed with

SPIN90 (top), subselection of particles used for Arp2/3-SPIN90 3D reconstruction (middle), and examples of 2D classes (bottom). **F.** Micrograph of Arp2/3 with SPIN90 and mDia1 (top), subselection of particles used for Arp2/3-SPIN90-mDia1 3D reconstruction (middle), and examples of 2D classes (bottom).

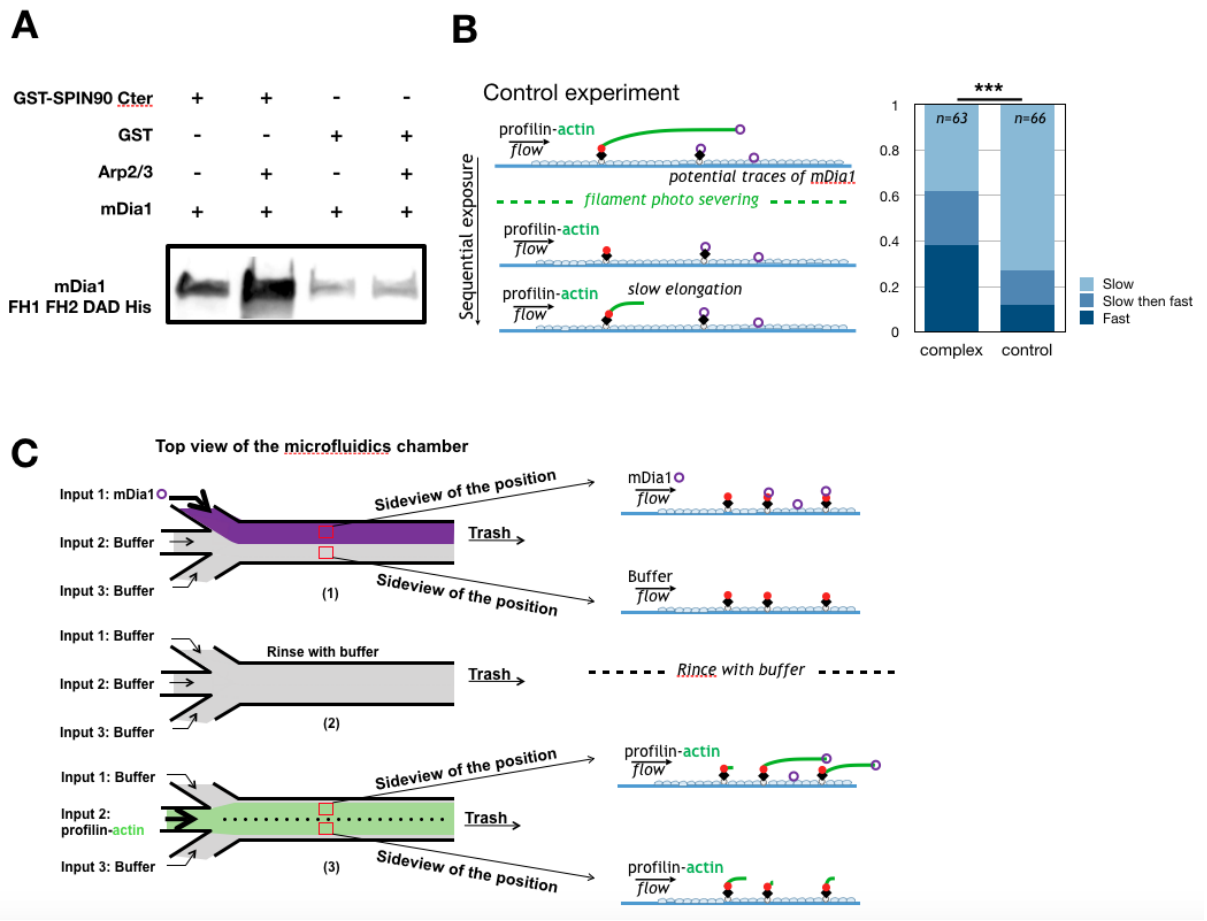

Fig S15 related to Figure 6: **A**. GST pull down assay (related to **Fig. 6A**). GST or GST-fused SPIN90 C-terminal coated beads were incubated without or with 540 nM Arp2/3 for 1 hour. The beads were washed three times with buffer before being incubated with 750 nM mDia1 FH1-FH2-DAD dimer for 1 hour. All the proteins attached to the beads were eluted with 20 mM GSH. The amount of mDia1 pulled down was detected with Anti His antibody by western blot. The left two bands show that the presence of Arp2/3 increases the binding fraction of mDia1 to GST SPIN90 C-terminal. The right two bands, as negative controls, show that mDia1 does not bind GST directly and that the presence of Arp2/3 does not increase the affinity of mDia1 for GST. **B.** Left: schematic diagram of a control experiment (related to **Fig. 6C-D**). Control experiments consist in observing the elongation of new, bare barbed ends growing in a microfluidics chamber with a SPIN90-decorated surface exposed to Arp2/3 and mDia1. This is achieved by first following the sequence shown in **Fig. 6C,** except that before profilin actin was injected into the chamber, the surface was subjected to a strong laser illumination (to be comparable to the "control"). Filaments are then photo-severed with a strong laser illumination (see Methods). Finally, we observe the regrowth of filaments from SPIN90-Arp2/3. The photo-severing ensured that the newly elongating barbed ends were initially without mDia1. The distribution of slow (light blue), slow then fast (blue), and fast (dark blue) filaments was compared to experiments like the ones presented in **Fig 6C-D** (bar charts, on the right). "Complex" denotes the experiments performed as in **Fig 6C-D** (with an additional exposure to light, to have the same conditions as in the control) and "control" denotes the control experiments. Comparison using Fisher's exact test: p=0.31 for the slow-then-fast population, and p=0.0013 for the fast population. **C.** Sketch detailing the observation of the mDia1-free population reported in **Fig 6E**. After the SPIN90-decorated surface was exposed to Arp2/3, we exposed only one half of the chamber to mDia1 (1): half of the chamber thus contained both SPIN90-Arp2/3 complex and SPIN90-Arp2/3-mDia1 complex, while the other half was decorated with SPIN90-Arp2/3 complex only. After rinsing with buffer (2), the surface was exposed to profilin-actin. In the region exposed to mDia1, filaments with different elongation rates appeared; while in the region that was not exposed to mDia1, only slow growing filaments were observed.

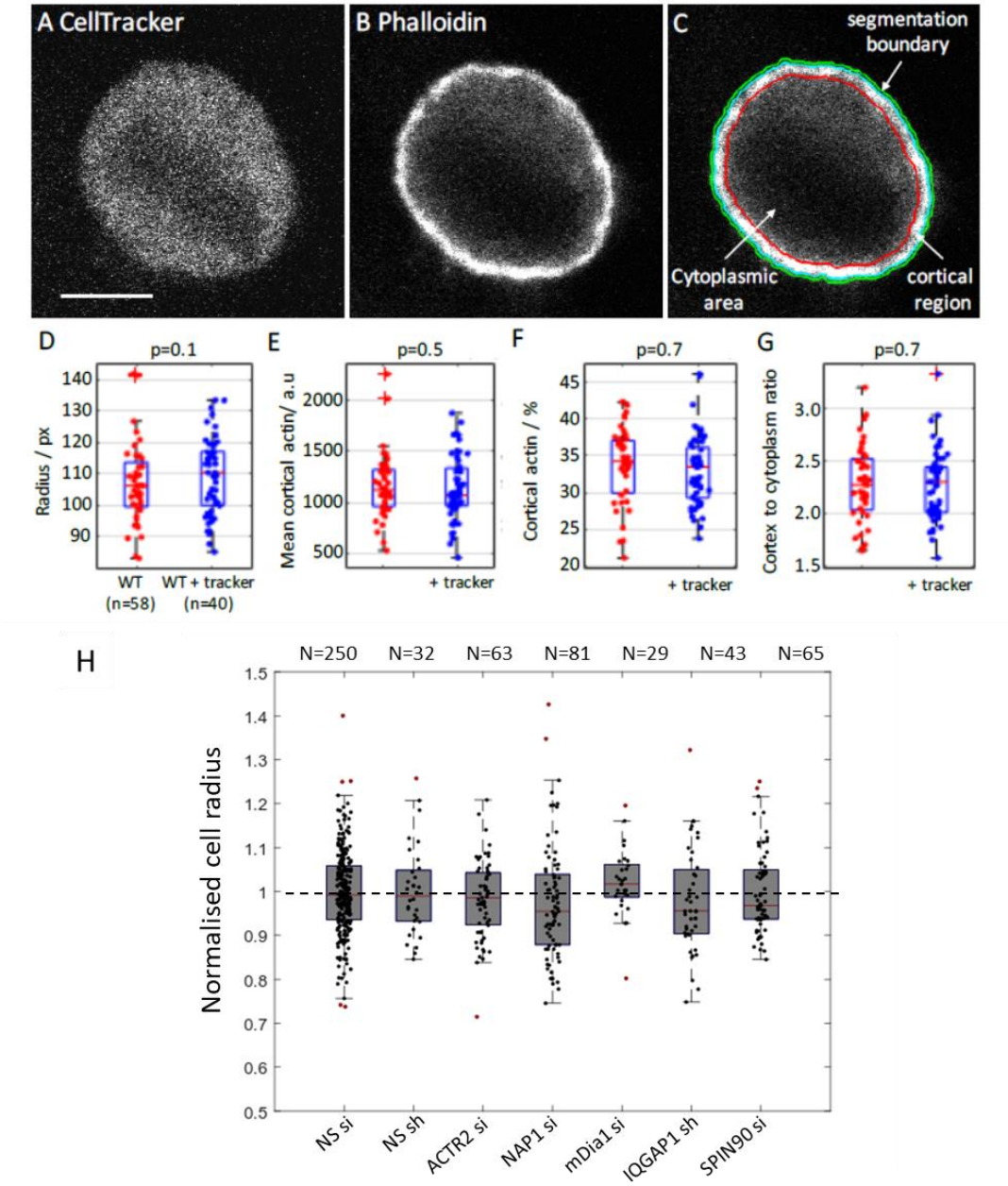

Figure S16 related to figure S6. A. Cells transfected with Non-Silencing siRNA or Non-Silencing shRNA were stained with CellTracker deep red. Representative image of a metaphase HeLa cell from a single optical section from a confocal microscopy stack. Scale bar=5µm. **B.** Same cell as in A stained with Phalloidin-Alexa 568 to reveal cortical F-actin. **C.** Representative segmented cell. The green line shows the boundary of the cell segmented from background. The red line shows the boundary between the cortex and the cytoplasm. The cortex is taken as the region contained between the green and red lines. The cytoplasm is the region within the red line. **D-G.** The radius, mean cortical actin, cortex to cytoplasm ratio, and percentage cortical actin of cells is not affected by labelling with CellTracker. **H.** The radius of cells is not affected by expression of shRNA. The radii of cells depleted in nucleators and NPFs is compared to non-silencing sh/siRNa (NS sh/si). The number of measurements are indicated above each box. **(D-H)** Data are plotted as box-whisker plots. Whiskers indicate minimum and maximum values. Data points are overlaid. Statistical outliers are indicated by red crosses (D-G) or red dots (H).

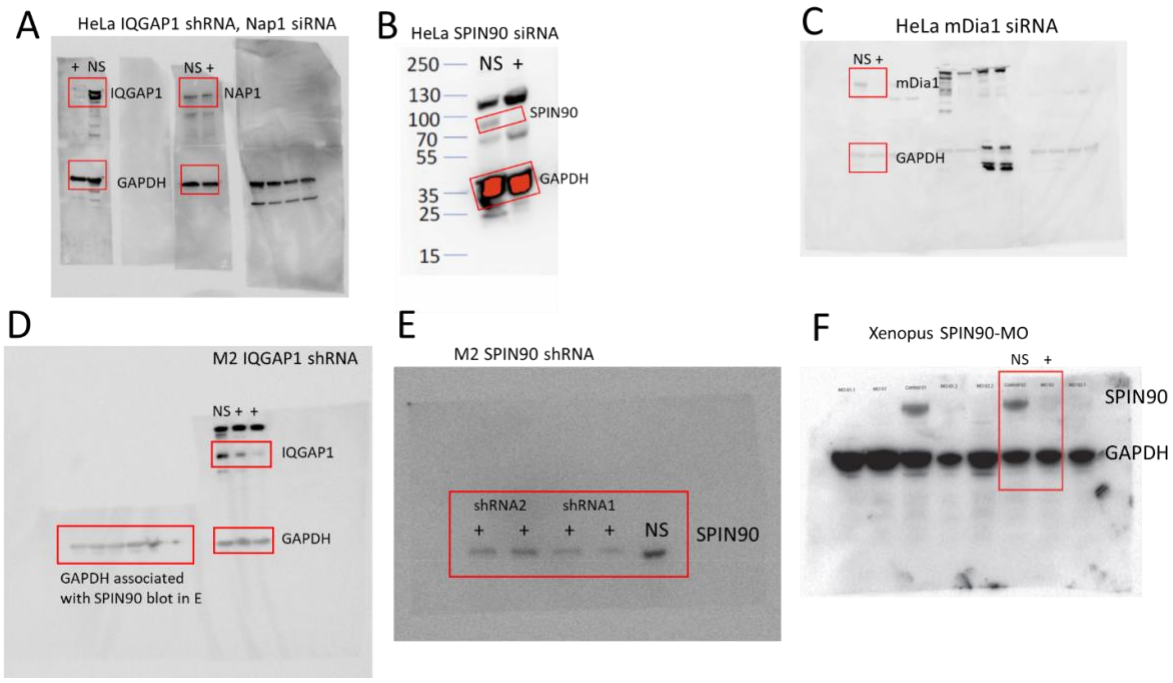

Fig S17: Uncropped Western blots. In all blots, the regions presented in figures are indicated by the red boxes. NS signifies non-silencing and '+' signifies that the targeting siRNA/shRNA/MO has been used. The treatments are indicated above each blot. **A.** Uncropped Western blot from Fig S3D and S3G. **B.** Uncropped Western blot from Fig S3F. **C.** Uncropped Western blot from Fig S3B. **D.** Uncropped Western blot from Fig S1F and G. **E.** Uncropped Western blot from Fig S1F. **F.** Uncropped Western blot from Fig S9A.

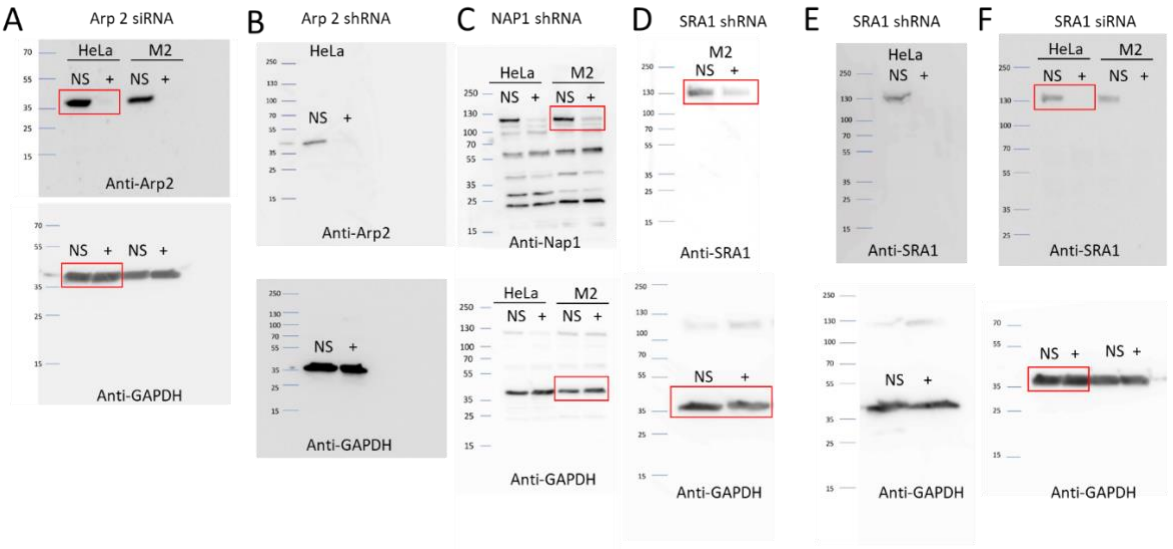

Fig S18: Uncropped Western blots. In all blots, the regions presented in figures are indicated by the red boxes. NS signifies non-silencing and '+' signifies that the targeting siRNA/shRNA has been used. The treatments are indicated above each blot. **A**. Uncropped Western blot from Fig S3C. **B**. Uncropped Western blot related to Fig S3A. **C**. Uncropped Western blot from Fig S1I. **D**. Uncropped Western blot from Fig S1H. **E**. Uncropped Western blot related to Fig S3A. **F.** Uncropped Western blot related to Fig S3E.

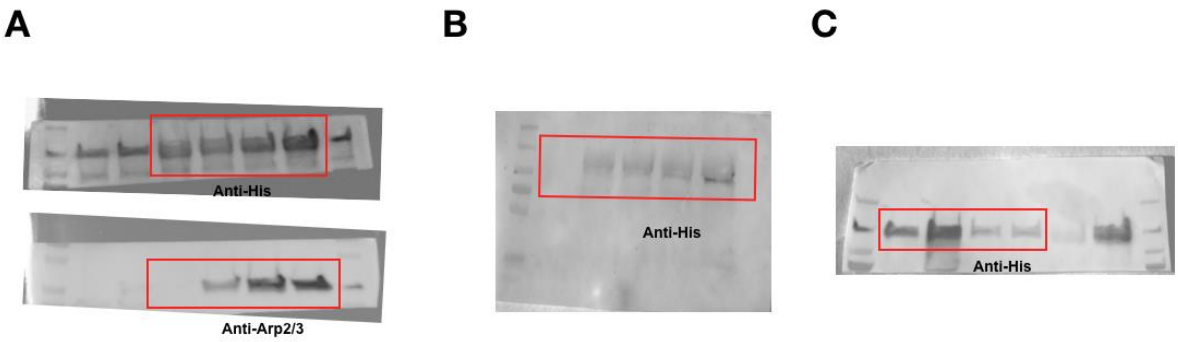

Fig S19: Uncropped Western blots related to in vitro assays. **A**. Uncropped Western blot from Fig 6A. **B**. Uncropped Western blot related to Fig S11C. **C**. Uncropped Western blot from Fig S14A.

Supplementary tables

Protein	Copy number	Copy number normalized to actin
Actin (all isoforms)	5.37E+07	1
RhoA	4.02E+06	0.075
mDia1	5.14E+05	0.010
Arp2/3 complex	1.24E+06	0.023
Wave complex	1.77E+05	0.003
SPIN90	8.09E+04	0.002
IQGAP1	2.44E+06	0.045
Profilin 1	2.18E+07	0.407

Table S1: **Copy number of proteins of interest per cell and copy number normalized to actin.** Data from proteomic studies on HeLa cells by Bekker et al[4]. For the Arp2/3 complex and the Wave complex, the copy number of the least abundant subunit was taken as an estimate of complex abundance.

Recent work has shown that the concentration of actin in a variety of cell lines is between 150 and 200 µM [5]. Assuming an actin concentration of his 150 µM, this allows us to estimate the concentration of nucleators and NPFs: mDia1: 1.4 µM, Arp2/3 complex: 3.5 µM, Wave complex: 500 nM, SPIN90: 250 nM, IQGAP1: 6.8 µM, Profilin 1: 61 µM. As a number of these proteins must be activated to play a part in nucleation and some are localized to the membrane while others are localized to the cytoplasm, the actual concentration of protein to include in in vitro assays is challenging to estimate.

	Phenotype	Observed number of cells in each category	Expected number of cells in each category based on control	P-Value (CHITEST)
CONTROL (non-silencing shRNA)	No blebs	15		
	Small blebs	54		
	Normal blebs	79		
	Large blebs	63		
IQGAP1 shRNA	No blebs	20	13	<0.001
	Small blebs	15	48	
	Normal blebs	45	71	
	Large blebs	109	56	
SPIN90 shRNA	No blebs	7	9	<0.001
	Small blebs	17	32	
	Normal blebs	45	47	
	Large blebs	56	37	
SRA1 shRNA	No blebs	8	3	<0.001
	Small blebs	24	10	
	Normal blebs	7	15	
	Large blebs	0	12	
NAP1 shRNA	No blebs	15	3	<0.001
	Small blebs	22	10	
	Normal blebs	3	15	
	Large blebs	0	12	

Table S2: Raw data and statistical analysis of the phenotypes in the shRNA blebbing screen
Cells stably expressing the shRNA construct of interest were categorized as normal, displaying large blebs, and displaying small blebs. For each targeting shRNA construct, observed distributions were compared to expected numbers based on the categorization observed in non-silencing shRNA control using a chi-square test. Differences were considered significant for $p<0.01$. Bleb size distributions were compared to those obtained for depletion of mDia1 and ACTR2 obtained in [2].

Supplemental Experimental Procedures

Cell culture and generation of cell lines

M2 melanoma cells were a kind gift of Prof Tom Stossel (Harvard Medical School, Boston, USA) and were originally described in [6]. Cell lines were cultured in MEM with Earle's salts and L-Glutamine (PAA) with penicillin/streptomycin, and 10% 80:20 mix of newborn calf serum/fetal bovine serum. M2 cells stably expressing the F-actin reporter Life-Act Ruby have been previously described in [2].

Wild-type HeLa cells were gift from the MPI-CBG Technology Development Studio (TDS). The stable HeLa GFP-Actin line and the HeLa Life-Act-Ruby line were described in [2]. HeLa cells stably expressing LifeAct-Ruby or GFP-actin were cultured in DMEM (PAA or Gibco) with penicillin/streptomycin, L-Glutamine, 10% fetal bovine serum and 750µg/ml G418. HeLa cells were arrested in prometaphase with 100nM Nocodazole (Merck Biosciences) for 16h for the localisation studies. For metaphase arrest in laser ablation and AFM studies, cells were treated for at least 1 hour with 10µM MG132 (Sigma, St Louis, MO, USA).

To obtain stable protein knock-down cell lines, M2 or HeLa cells (wild type or stably expressing LifeAct-Ruby) were transduced with lentiviruses encoding shRNA constructs targeting the genes of interest (see lentiviral shRNA generation and transduction). The cells were then selected with 250ng/ml puromycin for two weeks.

HEK293 cells stably expressing the SV40 large T antigen (HEK293T cells[7]) were cultured in DMEM supplemented with penicillin/streptomycin and 10% FBS. Cells were subcultured at a ratio of 1:5 and cultured similar to HeLa cells.

None of the cell lines used in this study were found in the database of commonly misidentified cell lines maintained by ICLAC and NCBI Biosample. All cell lines were cultured at 37C with 5% CO_2. All lines were routinely screened for the presence of mycoplasma using the mycoALERT kit (Lonza).

All imaging was done in Leibovitz L-15 media (PAA) supplemented with 10% fetal calf serum or in phenol-red-free DMEM (Gibco) supplemented with 10% fetal bovine serum, L-Glutamine and penicillin/streptomycin.

Plasmid construction and transfection

Full length human and mouse *SPIN90* were obtained from the Mammalian Gene collection or the I.M.A.G.E. library and cloned into EGFP-C1, EGFP-N1, or EBFP2-C1 vectors using restrictions sites inserted by PCR.

SPIN90, SPIN90-NT, and SPIN90-CT were described in [8]. IQGAP1-GFP was a kind gift from Prof David Sacks (NIH, MA, USA, [9]), the DBR domain of IQGAP1 tagged with GFP was a kind gift of Prof Robert Grosse (University of Marburg, Germany, [10]), and Fli-I-GFP was a kind gift from Prof Robert Tombes (Virginia Commonwealth University, VA, USA,[11]). Wave-2-GFP with a truncated CMV promoter to allow for speckling microscopy was a kind gift of Dr Orion Weiner (University of California San Francisco, USA,). EBFP2 was obtained from Addgene (plasmid 14893, [12]) and was substituted for EGFP in some constructs. All gene products were verified by sequencing.

cDNA was purified from bacteria using the Qiagen spin miniprep kit. Transfections were carried out using Lipofectamine 2000 according to manufacturer instructions. A typical transfection mixture for one well of a 6-well plate contained 1000µl Optimem (Invitrogen), 2.5µl Lipofectamine 2000 (Invitrogen), and 1µg of plasmid DNA.

Mass Spectrometry and Data Analysis

Mass spectrometry and data analysis were described in [2]. For data analysis, all proteins of the same family were grouped and isoforms of the same protein were considered as one. Two criteria were applied for considering a protein to be a reproducibly identified component of bleb cortex: 1) the presence of three or more sequence counts and a false positive protein identification rate of less than 1; 2) detection of the protein (using criteria 1) in at least two out of three replicate runs. To estimate the abundance of proteins in bleb cortex we rely on Protein Abundance Index (PAI) [13] in a modified form. PAI was calculated based on spectral count as follows: PAI = spectral count/MW, where MW corresponds to the protein molecular weight, which was used to adjust for differences between proteins in the number of observable peptides. The identified protein list was then curated for actin nucleation promotion factors.

Lentiviral shRNA production, transduction, constructs and targeted screen analysis

Lentiviral shRNAmir constructs in pGIPZ or pLKO.1 vectors targeting mDia1, ACTR2, ARPC2, SRA1, NAP1, SPIN90, Fli-I and IQGAP1, as well as non-silencing shRNA, were obtained from Open Biosystems (pGIPZ) or Sigma-Aldrich (pLKO.1).

The lentiviral constructs generated with the pGIPZ vector allow detection of transduced cells by expression of a GFP reporter contained in the vector. In some experiments, the GFP in the pGIPZ shRNAmir constructs was replaced with EBFP2 by using *SnaB*I and *BsrG*I sites. After initial selection with puromycin (250ng/ml for two weeks), this allowed the generation of cell populations with homogenous levels of knock down using flow cytometry. Cells transduced with shRNA in the pLKO.1 vector were selected on the basis of puromycin resistance alone. The shRNAmir construct gene accessions, oligo Ids, target sequences and transfection protocol are given in the next table. Target depletion was validated using qPCR or Western blotting.

<u>Lentiviral production:</u>

HEK293T cells were transfected with the lentiviral shRNA vector using the calcium phosphate transfection method. $2x10^6$ HEK293T cells were seeded in a T75 before transfection 4 hours later. Tube 1 contained HBS (NaCl (280mM), Na_2HPO_4 (1.5mM) and HEPES (50mM) in water at pH 7). Tube 2 contained $CaCl_2$ (2M), lentiviral plasmids (1.5µg pMDLg/pREE, 1.5µg pRSV-Rev and 3µg pMD2-VSVG) and 6µg of the shRNA plasmid of interest. The contents of tube 2 was added to tube1 drop by drop, and mixed gently. This transfection mix was then added to cells and incubated. The day after transfection, culture medium was replaced with fresh growth medium. After 48h, the supernatant was harvested and filtered through 0.45µm filters to remove all cell debris before transduction.

<u>Generation of stable knock-down lines:</u> Cells to be transduced were seeded into 10cm Petri dishes (HeLa cells: $2.5x10^5$ cells, M2 cells: $5x10^5$ cells). On the day of transduction, the cell medium was replaced by the viral supernatant together with 5µg/mL Hexametrine dibromide (Sigma) to aid viral entry. Host cells were left to grow for 3 days after transduction before selection with puromycin (1µg/mL). Western blotting and qPCR were used to confirm protein and mRNA transcript depletion.

Table S3 pGIPZ shRNA constructs. The columns of the table contain the name of the construct, accession number of the targeted gene, manufacturer's oligo ID, and the mature sense sequence of each construct used in the shRNA.

Construct	***Accession***	***Oligo ID***	***Sequence***
Non-silencing	*-*	*RHS4346*	*ATCTCGCTTGGGCGAGAGTAAG*
mDia1_22	*NM_001079812*	*V3LHS_392378*	*CAGATAGTTCTGCACAAGA*
ACTR2/Arp2_63	*NM_005722*	*V3LHS_341063*	TTCTTGGTACTCTTGTCGG
ACTR3/Arp3_82	*NP_005712.1*	*V3LHS_382341*	*TCGCTTCAACATGCCAGCT*
ArpC2_25	*NM_005731*	*V2LHS_199425*	ATTTCAAAGAAATACTGAC
IQGAP1_07	*NM_003870*	*V3LHS_334306*	*AGGTTGACTTCACAGAAGA*
SPIN90_95	*NM_016453*	*V3LHS_341595*	*TTCTCTTGCACATTTTCTT*
SPIN90_98	*NM_184231*	*V3LHS_341598*	*TCAGGAGCAACAACAGCTT*
Flightless-I_22	*NM_002018*	*V3LHS_386022*	*ACTGTGGAAGACACACACT*
CYFP1/Sra1_63	*NM_001324125*	*V2THS_258463*	*TTAATAATCTCATCTTTGC*
NCKAP1/Nap1_66	*NM_205842*	*V3LHS_347966*	*TATAGAGAAGCATAACTCA*
Wave2_14	*NM_006990*	*V2LHS_95114*	*TATCCTTGGTGTCCTGCAG*

Table S4 PLKO shRNA constructs (Human). The columns of the table contain the name of the construct, accession number of the targeted gene, manufacturer's oligo ID, and the mature sense sequence of each construct used in the shRNA.

Construct	***Accession***	***Oligo ID***	***Sequence***
PLKO (Empty)	-	SHC001	-
Flightless-I_63	NM_002018	TRCN0000152063	CCATTTCAAGAGGAAGTTCAT
Flightless-I_51	NM_002018	TRCN0000157051	GCTGCCACAGATCAACTACAA
IQGAP1_85	NM_003870	TRCN0000047485	CCAGTAATCTACATTTCCATT
IQGAP1_87	NM_003870	TRCN0000047487	GCATCCACTTACCAGGATATA
Nap1/NCKAP1_41	NM_013436	TRCN0000151941	CCTCTCAATCAAGATACTCAA
SPIN90_43	NM_016453	TRCN0000278443	CTAGAGGAGCTGCTGCATATT
SPIN90_72	NM_016453	TRCN0000141072	CTAGAGGAGCTGCTGCATATT

Flow cytometry

Flow Cytometry was carried out on a FACSAria III. Cells to be sorted were grown to full confluence in a T75 flask (~10^7 cells). Cells were resuspended in 1.5 ml of Gey's balanced salt solution (Sigma) and passed through a cell strainer (40µm mesh size). Cells were sorted using the appropriate laser for fluorescence activation of EGFP, EBFP2, or mRFP. Only the cells with the highest 5% fluorescence were collected. After sorting, the cells were resuspended in normal growth medium and amplified for use in experiments.

Stable cell line generation using linearized cDNA

Cell lines stably expressing a construct of interest were generated by linearising the cDNA with the appropriate restriction site. After lipofection, cells were selected with 1 $mg.ml^{-1}$ G418 for 2 weeks. To achieve a homogenous level of fluorescence expression, cells were sorted using flow cytometry. Cells expressing rescue constructs for IQGAP1 and SPIN90 knock-down were generated in this way.

siRNA depletion

For acute knockdown of proteins, cells were transfected with siRNA using Lipofectamine RNAiMAX according to manufacturer recommendations (Invitrogen, Life Technologies). siRNA stocks were made by resuspending siRNA in RNase-free buffer at a final concentration of 20µM. The Lipofectamine RNAi max reagent (Invitrogen) was used to transfect cells with siRNA (**Table S4**). siRNA was resuspended in RNase-free buffer at a final concentration of 20µM. Cells were generally used for experiments 72h after transfection except cells depleted for mDia1 which were used after 48h due to high cell death in response to depletion. All siRNA were used at 20 µM except Diaph1 siRNA and Nap1 siRNA which were used at half concentration (10 µM) due to the strength and lethality of their depletion. Knock-down

efficiency was verified by Western blotting and qPCR.

Table S5 siRNA ON-TARGETplus pool sequences (Human, GE Dharmacon), Diaph1 Stealth siRNA (Human, Thermo Fisher). The table indicates the name of the construct, the four target sequences contained in the pool, and the manufacturer's oligo ID for each siRNA pool.

Construct	***Target sequence***	***Oligo ID***
Non-silencing	UGGUUUACAUGUCGACUAA UGGUUUACAUGUUGUGUGA UGGUUUACAUGUUUUCUGA UGGUUUACAUGUUUUCCUA	D-001810-10-05 (GE-Dharmacon)
ACTR2/ARP2	GAAAGAGCAUUUAUCGUUU GAACAUGGAUCUUAGAGUC AGAAUGGAAUGGACUCUUA UGGUGUGACUGUUCGAUAA	L-012076-02-0005 (GE-Dharmacon)
mDia1	GGCUUCAAUAUCAGCUUCCUCUGUA	HSS102771 (Sigma)
IQGAP1	GAACGUGGCUUAUGAGUAC GCAGGUGGAUUACUAUAAA CGAACCAUCUUACUGAAUA CAAUUGAGCAGUUCAGUUA	L-004694-00-0005 (GE-Dharmacon)
SPIN90	GAGAAACGAGUUCGAGUCU GCACGCCUUUCGCCCAGUU CCGAGAAGCUGUUGUUGCU CGAGAGAUGUGCAAGGAAU	L-021376-00-0005 (GE-Dharmacon)
Flightless-I	UUAACAAGAAUGAGCGGAA ACGAAGACCUAGACGGCAU CCGGGAAGGUGAAACGCGA CAACCAGGGCAUCGUGUAU	L-017506-01-0005 (GE-Dharmacon)
Nap1/NCKAP1	CAUCCUAUCUUAUCGACAA GCAGACGACUUUAUAGAUA GGAGAAUGUUGAUGUGUUA GGUCGUAGCUCUUUCUUCA	L-010640-00-0005 (GE-Dharmacon)
Sra1/CYFIP1	GCACAAUCCUGCAGUACGU GGAGAGAAUUCGCAAGUUC GAUAAACGGUUACGAUCAG GAGUACGGCUCUCCUGGUA	L-014185-00-0005 (GE-Dharmacon)

Confocal microscopy

All fluorescence imaging (except for cortex ablation experiments) was performed using a 100× oil-immersion objective on an inverted microscope (IX81, Olympus) fitted with a spinning disk head (Yokogawa, CSU22). Images were acquired with an Andor iXon camera and analyzed using ImageJ (http://rsbweb.nih.gov/ij/) and Excel (Microsoft) software.

Excitation with a 488nm wavelength laser was utilised for GFP-tagged proteins, with a 543nm wavelength laser for mRFP-, Ruby-, and mCherry-tagged proteins as well as Alexa568-labelled antibodies, with a 405nm wavelength laser for EBFP2-tagged proteins, and with a 647nm wavelength laser for nucleic acids labelled with CellTracker deep red (Life Technologies).

Phenotypic blebbing screen

To quantify the impact of stable gene depletion on blebbing, cells stably transfected with targeting or non-silencing shRNA constructs were imaged and categorised as having normal, large, or small blebs. The effect of targeting shRNAs on cellular phenotype was assessed by comparing the experimentally observed number of cells in each category to that expected for control cells expressing non-silencing shRNA using Chi-square tests. Results were deemed significant for $p<0.01$ and are summarized in **Table S2.** For each shRNA, we verified that stable transfection led to a significant reduction in target mRNA transcript levels using qPCR and in protein levels using Western blotting.

To compare the effect of depletions, we computed a blebbing index for each condition compared to control:

$$Blebbing\ Index = 1 + \Delta_{Big\ blebs} - \Delta_{No\ blebs} - \Delta_{Small\ blebs}$$

With $\Delta_{Big\ blebs} = f_{Big\ blebs} - f_{Big\ blebs\_control}$ the change in the proportion of cells with big blebs compared to control, $\Delta_{No\ blebs}$ the change in the proportion of cells with no blebs compared to control, and $\Delta_{Small\ blebs}$ the change in the proportion of cells with small blebs compared to control. By definition, the blebbing index of the control population was 1.

Long term time-lapse imaging

To assess the impact of nucleator and NPF depletion on successful completion of the cell cycle, HeLa cells were imaged using long-term time-lapse imaging. To increase the proportion of mitotic cells, cells were first arrested in S phase with a single thymidine block by treatment with 2mM thymidine for ~16-24 hours. The block was released by replacing thymidine containing medium with normal DMEM medium ~7-8 hours before the start of imaging. For time lapse experiments, the cells were plated in 6-well plates, maintained at 37 C and supplied with 5% CO2 on the microscope stage. Multiposition long term time lapse microscopy was performed on a Zeiss axiovert 200M time lapse microscope using a 20X air objective (numerical aperture = 0.5). All experiments were performed in triplicate with at least 10-15 positions imaged per well. Experiments examining cell lines with stable shRNA depletion were plated the day before imaging. Experiments examining siRNA knockdowns were imaged beginning 48 hours after transfection. Time-lapse data was visualised using ImageJ and progression outcomes were tabulated and compared using Chi-square tests.

Drug treatments

CK666 (Tocris, Bristol, UK) [14] was used at 100µM to inhibit the Arp2/3 complex. SMIFH2 (Merck Biosciences) [15] was used at 40µM to inhibit formins. Cells were treated with drug for at least 30 minutes before starting measurements. For all drugs, an equal amount of DMSO was used as a vehicle control. All imaging was performed on at least three separate experimental days.

RNA extraction and Quantitative Real-Time PCR

Total RNA from M2 and HeLa cells was extracted using the RNeasy Mini Kit (Qiagen, Hilden, Germany) and reverse transcribed using the High Capacity cDNA Reverse Transcription Kit (Applied Biosystems, Carlsbad, CA) following manufacturer protocols. The gene expression level for endogenous controls *GAPDH* (Hs00266705) and *ACTB* (Hs00357333) was determined using pre-validated Taqman Gene Expression Assays (Applied Biosystems), and gene expression level for genes of interest was determined using assays designed with the Universal Probe Library (UPL) from Roche (www.universalprobelibrary.com) according to manufacturer's instructions. Sequences of primers used are available upon request. Gene expression was normalized to *ACTB* and *GAPDH* expression.

Scanning electron microscopy

Sample preparation for scanning electron microscopy was performed as described in [16] with minor modifications described in [2]. Two hours prior to sample preparation, whole cells were plated onto 12mm glass coverslips. Immediately prior to fixation, the coverslips were washed three times with L15 without serum and transferred to cytoskeleton buffer (50mM Imidazole, 50mM KCl, 0.5mM $MgCl_2$, 0.1mM EDTA, 1mM EGTA, pH 6.8) containing 0.5% Triton-X and 0.25% glutaraldehyde for 5 min. This was followed by a second extraction with 2% Triton-X and 1% CHAPS in cytoskeleton buffer for 5 min before washing the coverslips in cytoskeleton buffer three times. The remainder of the protocol was identical to [16]. The cells were dehydrated with serial ethanol dilutions, dried in a critical point dryer, coated with 5-6nm platinum-palladium and imaged using the in-lens detector of a JEOL7401 Field Emission Scanning Electron Microscope (JEOL, Tokyo, Japan). All samples were prepared in duplicate and images from two separate experimental days were acquired. Similar phenotypes were observed on both experimental days and images of at least 8 different cells were acquired for each experimental condition.

Scanning electron microscopy image analysis

Measurement of the cortical actin mesh size from scanning electron microscopy images was performed as in [1] from SEM images of blebs from M2 melanoma cells. Retracting blebs were excluded from the analysis and recognised on the basis of the characteristic crumpling of their surface [17]. Using a custom plugin developed in Fiji based on a trainable segmentation [1,18], pores were segmented in a semi-automated manner through intensity thresholding and size exclusion. From the final segmentation mask, the areas of holes were calculated and used to quantify the distribution of pore diameters. For this analysis, we utilised the scanning electron microscopy images acquired for cells in which NPFs had been depleted and cells from our previous study in which nucleators had been depleted [2].

Cortical thickness measurement

Measurement of the thickness of the actin cortex in metaphase HeLa cells was performed as described in [1]. Briefly, two-colour image stacks (30-70 z-slices, acquired at 100nm intervals) were acquired around the equatorial plane of rounded cells using a 60x colour-corrected objective (1.40 numerical aperture OSC2 PlanApoN) mounted on an Olympus FV1200 microscope. After correcting for chromatic shift and magnification using custom software written in MATLAB, a single equatorial plane was selected for each image using Fiji image analysis software. Cortex thickness and density were extracted as in [19]. For membrane width measurements, we measured the full-width at half-maximum of the plasma membrane intensity peak by interpolating the x position on the linescan on either side of the peak by linear interpolation of the two closest points. The half-maximum was defined as half of the difference between the peak intensity and intracellular background.

Imaging screen

To assess the localisation of NPFs in cells, we used the following imaging procedures sequentially until we were able to resolve localisation: i) transfection of GFP-tagged full length proteins, ii) simultaneous permeabilization and fixation of cells transfected with GFP-tagged full length constructs, iii) immunostaining when antibodies were available.

Immunostaining

For immunostaining, cells were fixed with 2% formaldehyde and 0.1% glutaraldehyde with 0.2% Triton X-100 in cytoskeleton buffer (50mM Imidazole, 50mM KCl, 0.5mM $MgCl_2$, 0.1mM EDTA, 1mM EGTA, pH 6.8) for 15 min at room temperature, washed three times with PBS. Non-specific binding was blocked by incubation in PBS supplemented with 10mg/mL BSA for 10min. The cells were then incubated for 60 min at room temperature with a monoclonal mouse anti-IQGAP1 antibody (1:100

dilution, WH0008826M1, Sigma), a monoclonal mouse anti-SPIN90 antibody (1:50 dilution, Santa Cruz, sc-514232), a polyclonal rabbit anti-SRA1 antibody (1:100 dilution, ab156016, Abcam), a polyclonal rabbit anti-NCKAP1 antibody (1:100 dilution, AbCam, ab96715), or a polyclonal rabbit anti-WASF2 antibody (1:50, a kind gift of Dr Alexis Gautreau, Ecole Polytechnique, France) diluted in PBS with 1% BSA. Cells were then washed three times with PBS/BSA and incubated with 1:100 Goat anti-rabbit or anti-mouse IgG Alexa 647 secondary antibody (Invitrogen) and 1:200 Alexa568-phalloidin (Invitrogen) to visualize F-actin for 60 min at room temperature. Finally the sample was washed four times with PBS/BSA. All samples were prepared in triplicate and images from two separate experimental days were acquired.

Phospho-MLC staining was carried out as above except that cells were first fixed for 15 minutes at room temperature with 4% paraformaldehyde diluted in a buffer containining 10mM MES, 138mM KCl, 3mM $MgCl_2$, 2mM EGTA. Then, after several washes with PBS, the cells were post-fixed with -20C acetone for 5 minutes. The rest of the protocol was as described above. Phospho-MLC was recognized with a monoclonal mouse anti-pMLC antibody recognizing phosphorylation on Ser19 (1:100 dilution, #3675, Cell Signalling).

Permeabilization-fixation for localisation of constructs in cells expressing GFP-tagged proteins

To remove fluorescence background due to cytoplasmic unbound proteins, we used a permeabilization-fixation approach. Permeabilization-fixation of cells was performed by replacing the imaging medium with 0.25% glutaraldehyde and 0.5% Triton X-100 diluted in cytoskeleton buffer while imaging the cells on a confocal microscope.

Western blotting

Cells were detached by trypsinisation, pelleted, resuspended in 500µL D-PBS and kept on ice for 3-5 min. Cells were then pelleted at 4C. The supernatant was discarded and cells were resuspended in lysis buffer containing protease inhibitors and PMSF (Santa-Cruz). After 3 minutes on ice, an equal volume of 2x Laemmli Buffer was added to the cell suspension. Samples were prepared for SDS-PAGE by boiling at 95C for 5 min. The level of protein depletion was assessed by Western blot analysis. Equal amounts of cell lysates were loaded on a polyacrylamide gel. Proteins separated on SDS-PAGE were transferred onto a PVDF membrane (pore size 0.45µm). Membranes were blocked with 5% non-fat dry milk in TBS-T for 1 h at room temperature and subsequently incubated overnight (at 4C) with the appropriate primary antibodies. The antibodies used for Western blot analysis and their dilutions are listed in table S5. After extensive washing with TBS-T, membranes were incubated with the appropriate HRP-coupled secondary antibodies (dilution 1:10000) for 1 h at room temperature. All secondary antibodies were from Jackson ImmunoResearch. After extensive washing with TBS-T, protein bands were visualised using ECL Detection kit (GE Healthcare) or SuperSignal West Femto (Thermo Scientific). All Western blotting was performed in duplicate.

Membranes were imaged with the CCD-based imaging ImageQuant LAS 4000 system. Images were taken in continuous intervals of 1 minute. A single image of the ladder was also taken as a reference. Images were analysed with ImageJ to determine relative protein concentration. Briefly, a rectangular region of interest was drawn around the protein band, and intensity in the box was measured using the integrated density (IntDen) function in Fiji. A second region of interest of the same dimensions was then used to measure the background intensity in a region of the blot image in an area devoid of any bands. The background intensity was subtracted from the protein intensity. This procedure was carried out for all the proteins of interest and normalized to the background-subtracted intensity of the corresponding GAPDH bands.

Table S6 List of primary antibodies used in Western blotting. Suppliers, dilution, and host species are also indicated.

Protein	***Product No & Vendor***	***Dilution***	***Species***
GAPDH (control)	*NB300-221, Novus Biological*	*1:10000*	*Mouse*
mDia1	*Ab96784, Abcam*	*1 :200*	*Rabbit*
Arp2	*sc-10125, Santa Cruz*	*1:100*	*Goat*
Arp3	#4738, *Cell Signalling*	*1:200*	*Rabbit*
IQGAP1	*WH0008826M1, Sigma-Aldrich*	*1:200*	*Mouse*
SPIN90	*ab88467, Abcam*	*1:500*	*Mouse*
Nap1/NCKAP1	*ab96715, Abcam*	*1:500*	*Rabbit*
Sra1/CYFP1	*ab156016, Abcam*	*1:1000*	*Rabbit*
Flightless-I	*ab108594, Abcam*	*1:1000*	*Rabbit*

Quantification of cortical pMLC fluorescence

To determine relative levels of cortical pMLC fluorescence in control metaphase HeLa cells and cells depleted for a nucleator or an NPF, we acquired confocal microscopy images and segmented the cortex from the cell body using image analysis. Two cell populations were prepared, one transfected with targeting siRNA and the other with non-silencing siRNA. After 48h, the control population was marked with a fixable far red cytoplasmic marker according to manufacturer protocol (CellTracker Deep Red, Thermofisher Scientific). Then, the two populations were trypsinised and resuspended. 55,000 cells of each population were plated together onto a 13mm coverslip and left to adhere. The cells were then treated with Nocodazole overnight (100nM, Sigma). The next morning, two hours prior to fixation, the medium was replaced with medium containing MG132 (10µM) to enrich for cells in metaphase. Cells were then fixed and stained for pMLC. Cells were imaged using a 100x, 1.4NA oil immersion objective lens mounted on a FV1200 scanning laser confocal microscope (Olympus, Germany). Cells in metaphase were identified by their DNA morphology visualised with Hoechst 33342 stain. z-stacks were acquired with a 0.5µm interval between sections and a 4x zoom. At least 20 cells from each population were imaged.

To quantify the amount of cortical pMLC in each cell, the cell cortex was segmented from background using KoreTechs[20]. The cortical region was then defined as a region of fixed thickness (10 pixels) around the cell contour. This computed the mean cortical pMLC fluorescence intensity for each cell. We then computed the ratio of mean fluorescence in the targeting siRNA cells to NS siRNA cells. We used NS siRNA as a consistent control to compare cortical pMLC enrichment across experimental conditions.

Actin regrowth speed analysis

The rate of actin accumulation during cortex regrowth was measured as detailed in [20,21]. Blebs were induced by exposure of a small region of the cortex of metaphase HeLa cells expressing LifeAct-Ruby

to UV pulses. Following induction, blebs grow rapidly before stopping and eventually retracting. Actin is initially absent from below the bleb membrane but progressively accumulates as growth slows and retraction starts. To allow for reliable segmentation of the cell contour for subsequent image analysis, we added 2.5µM Alexa568 dye to the extracellular medium. Images were then processed, automatically analysed and visualised using KoreTechs. This allowed segmentation of the cortex from the cytoplasm and segmentation of the induced bleb from the rest of the cell body. Cortical and cytoplasmic fluorescence intensities of actin could then be monitored in the bleb and compared to the cell body control value. This analysis yielded curves relating the evolution of the actin fluorescence intensity in the bleb normalised to the cortical fluorescence intensity in the cell body. Actin accumulation in the cortex displayed two markedly different phases: the first started immediately after laser ablation and ended shortly after the cessation of growth; the second started after growth had finished and ended after bleb retraction (**Fig 2G**). Actin accumulation was approximately linear in both regimes and slopes relating the percentage actin accumulation per second could be measured by fitting straight lines to each interval.

Atomic Force Microscopy and Data Analysis

Indentations of cells by AFM were performed using a JPK NanoWizard-1 AFM (JPK, Berlin, Germany) mounted on an inverted microscope (IX-81, Olympus, Berlin, Germany). The day prior to experimentation, cells were plated onto 35mm glass bottom Petri dishes. Cells were incubated in MG132 (10µM, Sigma) for 2 hours prior to measurement to arrest cells in metaphase. Experiments were performed at room temperature and cells were maintained in Leibovitz L15 medium (Life Technologies) supplemented with 10% FBS (Sigma-Aldrich) and MG132 (10µM). Before each experiment, the spring constant of the cantilever was calibrated using the thermal noise method implemented in the AFM software (JPK SPM). The sensitivity of the cantilever was measured from the slope of force-distance curves acquired on glass. For apparent stiffness measurements, we used soft cantilevers with V-shaped tips (BioLever OBL-10, Bruker; nominal spring constant of 0.006 N m^{-1}).

For each measurement, the cantilever was first aligned above a metaphase cell using the optical microscope. Then, force-distance curves were acquired over the center of the cell at the 4 vertices of a square with a 2µm side. At each of these four positions, up to 10 curves were acquired with an approach speed of 2.5µm.s^{-1} and a target force of 2.5nN. Force-distance curves were then post-processed to compute an apparent stiffness. First, we determined the contact point between the cantilever tip and the cell using the method outlined by Crick and Yin[22] implemented in MATLAB (MathWorks, Natick,MA, USA). The indentation depth was then calculated by subtracting the cantilever deflection *d* from the piezo displacement beyond the contact point *z* (δ=z-d). The resultant force-indentation curves were then averaged over each position and fitted with the Sneddon model to calculate each location's apparent elasticity [23]. Curve fitting was restricted to indentation depths shallower than 500nm to maximise contributions of the cortex to the restoring force and minimise contributions from the cytoplasm [24].

Xenopus embryo manipulation

Xenopus embryos were obtained as previously described [25,26]. Briefly, ovulation was induced in adult females by injecting serum gonadotrophin (Intervet) followed by injection of human recombinant chorionic gonadotrophin (Intervet). After ovulation, oocytes were collected and used for *in vitro* fertilization. Fertilizations were carried by mixing oocytes with a sperm solution obtained from adult testicles. Embryo stages were determined by following previously published *Xenopus* developmental stage series[27]. All animal experiments complied with the Biological Service Unit at University College London and UK Home Office guidelines (Animal Act 1986).

mRNA transcription

Templates for nuclear-RFP (nRFP) and membrane-GFP (mGFP) mRNA transcription were generated by linearizing plasmids containing coding sequences for these tags with the restriction enzyme NotI (Promega). mRNA transcription was performed by using the mMESSAGE mMACHINE SP6 Transcription Kit according to manufacturer instructions (Thermo-Fisher, AM1340).

Xenopus morpholino microinjections and rescue experiments

Microinjections were done using calibrated glass needles as previously described [25,26]. Jelly was removed from fertilised eggs by incubating for 5 min with a solution containing 2g of cysteine (Sigma) and 4 mL of 2.5N NaOH in 100 mL of Milli-Q H_2O. Injections were targeted to the 2 ventral blastomeres at the 4–8 cell stages. Blastomere labelling was achieved by injecting 10 nL of a mix containing nRFP or mGFP mRNAs (250 pg per blastomere of each construct). SPIN90-MO (5'-GTCCCTTCTGCCGCAACGCAAC-3') was synthesised by GeneTools (GeneTools, OR, USA) and co-injected at 40 ng per blastomere along with nRFP and mGFP. A standard non targeting was used as a control (GeneTools, OR, USA).

For rescue experiments, cDNA encoding Human SPIN90 tagged with EBFP2 was co-injected at 500 pg per blastomere along with a mix containing SPIN90-MO, nRFP and mGFP mRNAs. This Human version of SPIN90 is highly conserved with its *Xenopus* ortholog but is not targeted by the SPIN90-MO (**Fig S9**).

Western blotting from Xenopus embryos

Western blots were performed as previously published with minor modifications[25,28]. Briefly, whole embryos were homogenized in lysis buffer (20 mM Tris, 100 mM NaCl, 0.01% Triton-X, pH 8.0) complemented with protease inhibitor (Roche 11836153001). After homogenization, 100 µg of protein extract was loaded per lane of 4–12% polyacrylamide gels (Thermo-Fisher, NP0321). Proteins were transferred onto PVDF membranes (SIGMA, GE10600101) in a semidry system for 28 min at 10 mV. Membranes were blocked with 5% blocking reagent (Bio-Rad, 1706404) in TBS-T (TBS buffer and 0.1% Tween-20) for 1 hour and incubated overnight at 4C with a polyclonal rabbit anti-SPIN90 antibody (Abcam ab128154), used at 1:500 dilution in a solution containing 2.5% blocking reagent. Membranes were washed 5 times with TBS-T and then incubated with an anti-Rabbit HRP-conjugated secondary antibody (SIGMA, GENA934-1ML). Excess secondary antibody was removed by washing 5 times with TBS-T. Signal was revealed by chemiluminescence (WBLUF0100, Merck-Millipore) in a ChemiDoc XRS+ System (Bio-Rad). Western blot band intensity was acquired with ImageJ, normalised in Excel (Microsoft) and plotted in Prism7 using the methods described in [28]. Re-probing for α-Tubulin was performed by following standard soft stripping protocols[28], mouse α-Tubulin antibody was used 1:1000 dilution (DSHB, clone 12G10) and a secondary anti-Mouse-HRP antibody (SIGMA, GENA931-100UL) was used for detection.

Xenopus embryo staining, imaging, and cell area measurement

Phalloidin (Thermo-Fisher, A12379) staining was done as previously described [26]. Briefly, whole embryos were fixed with 4% PFA and 0.25% Glutaraldedyde in PBS containing 0.3% Triton-x100 for 15 min and washed 3 times in PBS-0.3% Triton-x100 for 10 min. After blocking with 10% normal goat serum for 10 minutes, embryos were incubated with 5U of phalloidin per mL in PBS-0.3% Triton-x100. Embryos were washed with PBS-0.3% Triton-x100 and dehydrated in Isopropanol (20 min) for clearing and mounting in BB:BA 2:1 (Benzyl-benzoate:1 Benzyl-alcohol, Sigma).

Images of F-actin localisation were acquired on an inverted confocal microscope (FluoView FV1000, Olympus) using either a 20x objective (UPLSAPO 20x/0.75 FWD = 0.6 mm, Olympus) or a 60x objective (UPLSAPO 60x/1.35 FWD = 0.15 mm, Olympus).

For cell area comparison across conditions, cells were manually segmented from images and their areas were calculated using FiJi.

Electron microscopy and single particle analysis

Concentrated mixtures of either Arp2/3-mDia1, Arp2/3-SPIN90, or Arp2/3-SPIN90-mDia1 were diluted and applied to freshly glow-discharged 300 mesh carbon-coated copper grids at final concentrations 22 nM Arp2/3, 100 nM SPIN90, 50 nM mDia1. The samples were negatively stained with uranyl formate 1%. Data were collected with a FEI tecnai G2 transmission electron microscope equipped with a LaB_6 emission filament operating at 200 kV. Images were captured on a TVIPS F416 CMOS camera at 50,000x magnification and 1.5 - 2.5 µm underfocus. The pixel size used was 2.13 Å/pixel. Using the CTF estimations from CTFFIND[29], micrographs were phase flipped.

Particles were hand-picked using XMIPP3 software from the image processing framework SCIPION[30]. Particles whose size would correspond to that of a potential complex incuding Arp2/3 were selected. 7572 particles were selected for the mixture of Arp2/3-mDia1; 6568 for the mixture of Arp2/3-SPIN90; 10 044 particles for the mixture of Arp2/3-SPIN90-mDia1. 2D class averages were obtained in Relion-3.0 [31]. Particles belonging to blurred averages were excluded from further analysis.

3D classification was performed to sort out 3 classes using Relion-3.0. Low-pass filtered crystal structures were used as references (low-pass filter: 40 Å). The crystal structure of Arp2/3●SPIN90 complex[32] (PDB : 6dec) was used for Arp2/3-SPIN90 data analysis. Different models generated from Arp2/3●SPIN90 complex (PDB: 6dec) and FH2 domains from Bni1p●actin complex[33] (PDB: 1y64) were used for Arp2/3-SPIN90-mDia1 data analysis. Arp2/3 crystal structure[34] (PDB: 4xf2), with and without FH2 domains from Bni1p●actin complex (PDB: 1y64), were used for Arp2/3-mDia1 data analysis. The particles belonging to the 3D class displaying the best fit to the model complex used as reference were selected for further processing while the divergent ones were left out.

These sorted particles were then used to reconstruct a 3D model with Relion-3.0 using strongly low-pass filtered references to prevent any bias (low-pass filter: 50-60 Å). The resulting 3D reconstructions shown in **Fig 6B** and **Fig S14** have a resolution of 27 Å both for Arp2/3-mDia1 data (5456 particles used), Arp2/3-SPIN90 data (4690 particles used) and Arp2/3-SPIN90-mDia1 data (2006 particles used). To interpret the resulting 3D reconstructions the non-filtered crystal structures used as references were fitted in the corresponding 3D maps using UCSF Chimera[35]. Spurious noise from EM densities was hidden with « Hide Dust » command from UCSF Chimera to facilitate readability.

Proteins purification for in vitro experiments (used in Fig. 4- 6, S10-S15)

Recombinant mouse GST tagged formin mDia1 (GST-FH1-FH2-DAD) was expressed in E.Coli Rosetta 2 (DE3) for 16h at 18C. GST-mDia1 was purified by affinity chromatography over a Sepharose 4B GSH affinity column (GE healthcare) followed by gel filtration over a Hiload Superdex 200 column (GE healthcare). The same method was used to purify recombinant GST-tagged human SPIN90 full-length (1-722) and GST-tagged SPIN90 C-terminal fragment (SPIN90 Cter, 267-722). No difference was observed between SPIN90 full-length and SPIN90 Cter in experiments performed with either construct: pyrene assays (**Fig S10A-D**) and ternary complex experiments performed in microfluidics (**Fig. 6C-E**). Other microfluidic experiments were performed with either SPIN90 Cter (**Fig. S11A**) or full length (**Fig. S11B**, **Fig. S10F**). All experiments in open chambers (**Fig. 4A-F**, **Fig. 5**, **Fig. S12**, **Fig. S13**) were performed with SPIN90 Cter. SPIN90 Cter-568 was labeled with Alexa Fluor 568 C5 Maleimide [36].

Recombinant mouse formin mDia1 (SNAP-FH1-FH2-DAD-His tag) and human profilin1 were expressed and purified following the protocol described [3]. mDia1-549 was labeled with SNAP-Surface 549 [37]. Arp2/3 was purified from sheep brain [38]. Skeletal muscle actin was purified from rabbit muscle acetone powder following the protocol described in [39]. SPIN90-647 was labeled with SNAP-Surface 647 [36].

Pyrene-actin assembly assay (Fig. S9A-D)

Actin assembly were detected by the change in pyrenyl-actin fluorescence in a Safas Xenius spectrofluorimeter (Safas) at room temperature. MgATP-G-actin (5% pyrene labeled), either 5 nM mDia1 or 20 nM Arp2/3 and various concentrations of SPIN90 (full-length or C-terminal construct) were mixed in G buffer (2 mM Tris HCl pH 7.8, 0.2 mM ATP, 0.1 mM CaCl2, 1 mM DTT). Polymerization is started by adding 8µL 20xKME buffer (4 mM EGTA, 20 mM MgCl2, 400 mM KCl) to the 152 µL reaction solution.

Single filament assays – microfluidics (Fig. 5C, Fig. 6C-E, Fig. S11, Fig. S13CD, Fig. S15BC)

Microfluidics experiments were done with Poly-Dimethyl-Siloxane (PDMS, Sylgard 184, Dow-corning) devices with dimensions of 60 µm x 800 µm x 1 cm, based on original protocols from [40]. The devices are cross-shaped consisting of channels with three inlets and one outlet. Flows were controlled and monitored by an MFCS and Flow Units (Fluigent, France). PDMS chambers were cleaned and mounted by following the protocol described in [3]. Single filament experiments were performed in F-buffer (5 mM Tris-HCl pH 7.8, 1 mM MgCl2, 0.2 mM EGTA, 0.2 mM ATP, 10 mM DTT, 1 mM DABCO, 50 mM KCl, and 0.1% BSA).

<u>Measuring filament nucleation and elongation by SPIN90-Arp2/3</u>

To specifically anchor GST-SPIN90 by its GST tag to the coverslip surfaces, clean surfaces were first incubated with a mixture of BSA and biotinylated BSA, then incubated with neutravidin (20 µg/mL) for 5 minutes and rinsed. Surfaces were exposed to 2 µg/mL biotinylated anti-GST (Rockland) and rinsed, then exposed to 250 nM SPIN90 for 5 minutes and rinsed.

To measure the SPIN90-Arp2/3 nucleation rate (**Fig. S11A**), a GST-SPIN90-decorated surface was exposed to 30nM Arp2/3 complex for 5 minutes and rinsed, then exposed to 0.5 µM 15% Alexa-488 actin and 0.5 µM profilin.

<u>Measuring filament nucleation, elongation, and processivity by SPIN90-mDia1</u>

When the anti-GST anchored surface was exposed to 50 nM mDia1 for 5 minutes and rinsed before being exposed to 1 µM 15% Alexa-488 actin for nucleation, only one filament was observed per field of view in 30 minutes observation. This showed that unspecific binding of functional mDia1 to the surface is very low. When the same surface was exposed to 250 nM SPIN90 for 5 minutes at first, then exposed to 50 nM mDia1 for 5 minutes and rinsed, and finally to 1 µM 15% Alexa-488 actin, about 126 filaments were observed per field of view during 30 minutes observation. Afterwards, those filaments were incubated with 0.5 µM unlabelled actin and 3.5 µM profilin, 17 of these barbed end anchored filaments were chosen randomly and their elongation rate was measured. The elongation rate of filaments by mDia1 in the absence of SPIN90 was measured on the same day and with the same actin and profilin concentrations. In these experiments, mDia1 was anchored to the surface as described previously [3].

The processivity of mDia1 (**Fig. S10F**) was measured on filaments anchored by their pointed ends to the coverslip surface, using spectrin-actin seeds. The presence of mDia1 at their barbed ends was assessed by their rate of elongation from profilin-actin. Thus the departure of mDia1 from the barbed

end was detected by an abrupt reduction of the elongation rate [3]. The solution contained 0.5 µM 15% Alexa-488 actin, 3.5 µM profilin, and 0 or 100 nM SPIN90.

Measuring mDia1's affinity for actin filaments nucleated by SPIN90-Arp2/3 and by spectrin-actin seeds (**Fig 5C, Fig. S13C)**

To specifically anchor GST-SPIN90-Arp2/3 and spectrin-actin seeds to the coverslip surfaces, clean surfaces were exposed sequentially to spectrin-actin seeds (2.5 pM, 5 minutes) and rinsed, neutravidin (20 µg/mL, 5 minutes) and rinsed, biotinylated anti-GST (Rockland, 2 µg/mL, 5 minutes) and rinsed, and SPIN90 (250nM, 5 minutes) and rinsed. 0.7 µM 15% Alexa-488 actin was flowed into the chamber for 5 minutes. All the actin filaments that appeared during this time were identified as being nucleated by spectrin-actin seeds. Afterwards, the surface was incubated with 30nM Arp2/3 complex for 5 minutes and exposed to 0.7 µM 15% Alexa-488 actin again to generate SPIN90-Arp2/3 nucleated filaments. Both SPIN90-Arp2/3 and spectrin-seeds nucleated actin filaments, which were anchored within the same fluidics chamber and homogenously distributed, were exposed to 0.4 nM mDia1, 0.5 µM 15% Alexa-488 actin and 3.5 µM profilin at the same time to compare mDia's affinity for each filament type (**Fig 5C, S13C**).

To measure mDia1's affinity for actin filaments with different lengths (**Fig S13D**), spectrin seeds were attached to the coverslip surface. After the surface was passivated with 3% BSA, 0.7 µM 15% Alexa-488 actin was flowed into chamber to generate actin filaments. Then, the surface was briefly exposed to 100% laser power, which may sever filaments. This yielded a surface with filaments with a broad length distribution anchored to it. These filaments were then exposed to 0.4 nM mDia1, 0.5 µM 15% Alexa-488 actin and 3.5 µM profilin simultaneously to compare mDia's affinity for long and short filaments.

Measuring filament nucleation and elongation by SPIN90-Arp2/3-mDia1

To grow filaments from the ternary complex of SPIN90-Arp2/3-mDia1 (**Fig. 6C-E**), a GST-SPIN90 (full-length or Cter construct)-decorated surface in a microfluidic chamber was first exposed to 40nM Arp2/3 complex for 2 minutes and rinsed, followed by exposure to 10 nM (or 50 nM) mDia1 for 30 seconds. The surface was then rinsed with buffer for 2 minutes before being exposed to profilin-actin (0.5 µM 15% Alexa-488 actin and 0.5 µM profilin). The nucleation and the elongation rates of the observed filaments were monitored.

To compare the nucleation rates of SPIN90-Arp2/3 complex with and without mDia1, after a GST-SPIN90 decorated surface in a microfluidic chamber was exposed to 40nM Arp2/3 complex for 2 minutes and rinsed, we exposed only half of the chamber to 50 nM mDia1 by manipulating the input pressures in our microfluidic device. The surface was then rinsed with buffer for 2 minutes before being exposed to 0.5 µM 15% Alexa-488 actin and 0.5 µM profilin (**Fig. S15C**). The nucleation and the elongation rates of the observed filaments were monitored (**Fig. 6E**). The fact that the nucleation rate of slow filaments is the same as in independent control experiments indicates that mDia1 dissociation from the ternary complex is negligible over the course of the experiment (otherwise we would have a significant portion of delayed nucleation of slow filaments). We are thus confident that the nucleation rate we measure for population (iii) is an accurate estimate of the actual nucleation rate of the ternary complex.

Nucleation and elongation by SPIN90-Arp2/3-mDia1: control experiments (**Fig. S15B**)

To estimate the contribution of potential traces of mDia1 on the surface (either due to non-specific binding or to interaction with anchored SPIN90) to the rapid elongation of filaments, the same surface

conditions were generated by exposing the GST-SPIN90-decorated surface to Arp2/3 and mDia1. Filaments were then nucleated by exposing the surface to profilin-actin for 20 seconds, and the chamber was then rinsed for 2 minutes. During these 2 minutes, the laser intensity was increased in order to sever the filaments, and these were rinsed out by the flow. Afterwards, the chamber was again exposed to the profilin actin solution to generate new barbed ends from the same, bare SPIN90-Arp2/3 complexes. Their elongation rate was monitored, and the rapidly growing population was greatly reduced compared to the experiment (**Fig. S15B**), indicating that these filaments did not result from the capture of mDia1 by the growing filament barbed ends. In contrast, the slow-to-fast growing population was not significantly reduced, indicating that part of them may have resulted from the capture of mDia1 by the growing filament barbed ends.

In order to determine if mDia1 (either adsorbed on the surface, or bound to SPIN90 or SPIN90-Arp2/3) was damaged by the strong exposure to light during the severing of the filaments in the control, the experiment (where filaments were not severed) was also performed with exposure to the same amount of light. To do so, we exposed the GST-SPIN90-decorated surface sequentially to 40 nM Arp2/3 for 2 minutes and to 50 nM mDia1 for 30s. The chamber was then rinsed with buffer for 2 minutes; during this time, the laser intensity was set to 100% (same conditions as in the control experiment, except that no filaments have elongated yet). Then, the chamber was exposed to 0.5 µM 15% Alexa-488 actin and 0.5 µM profilin. The elongation rates of the filaments generated in the first 5 minutes were monitored (Fig. S15B, 'complex'). The proportion of fast-growing filaments was comparable to the experiment without the strong exposure to light, indicating that the light did not damage the formins.

GST pull down assay to detect protein protein interaction (**Fig. 6A, S11C, S15A**)

First, glutathione beads (Glutathione Sepharose 4B, GE Healthcare) were incubated with 5% BSA for 5 minutes and washed 3 times with 500 µL GST pull down buffer containing 50 mM Tris-HCl pH 7.5, 1 mM DTT, 50 mM KCl, and 5% glycerol.

Investigating the binding between SPIN90 and mDia1

To investigate direct binding between SPIN90 and mDia1, we carried out a pull down assay with mDia1 anchored to glutathione beads. 50 µL 7.7 µM beads decorated with GST or GST mDia1 was mixed with 2.5-20 µM His-tagged SPIN90 full-length for 1 hour at 4C. The beads were washed by adding 500 µL GST pull down buffer. After centrifugation at 500 x g for 1 minute, the supernatant was discarded. After the washing steps were repeated three times, proteins attached to beads were eluted with 50 µL 20 mM GSH. The sample was separated by SDS-PAGE for western blot analysis (**Fig S11C**). The amount of SPIN90 pulled down was detected by anti-His antibody (QIAGEN).

Detecting formation of a ternary complex of SPIN90-Arp2/3-mDia1

To investigate formation of a ternary complex between SPIN90, the Arp2/3 complex, and mDia1, we carried out a pull down assay with SPIN90 anchored to glutathione beads. 50 µL 12 µM Glutathione Sepharose 4B decorated with full length GST SPIN90 was mixed with 0-540 nM Arp2/3 for 1 hour at 4C. After washing 3 times with 300 µL GST pull down buffer, these beads were further incubated with 700 nM His-tagged mDia1 dimer for 1 hour at 4C. After washing the beads 3 times with 300 µL GST pull down buffer, proteins attached to beads were eluted with 50 µL 20 mM GSH. The sample was separated by SDS-PAGE for western blot analysis. Anti-His antibody (QIAGEN) and anti-ArpC2 (Sigma)

were used to detect His-tagged mDia1 and Arp2/3. Membranes were imaged with ImageQuant LAS-4000 mini imaging system. The amount of mDia1 pulled down was quantified by ImageJ (**Fig 6A**).

The control experiment (**Fig S15A**) was done in the same way except the first step: 50 µL 12 µM Glutathione Sepharose 4B decorated with GST or GST SPIN90 Cter was mixed with or without 540 nM Arp2/3 for 1 hour at 4C.

Single filament and network assays – open chambers (Fig. 4A-D, 5A-B, 5D, 6F-G, S12, S13A-B)

Coverslips were passivated with mPEG silane following the protocol described in [41]. Strips of parafilm were affixed to the cover glass to form individual, linear flow chambers. The cover glass was heated to slightly melt the parafilm. Then, a passivated coverslip was stuck on top of the cover glass to generate flow chambers. To observe single molecules of labeled mDia1 and labeled SPIN90, the mPEG silane-passivated flow chambers were incubated with 1 mg/mL PLLPEG for 5 minutes to further improve the passivation. The open flow chamber experiments were performed in F-buffer with 0.2% methylcellulose. As full-length SPIN90 appeared to be very sticky in the open flow chamber, SPIN90-Cter was used in these assays.

Filament networks (**Fig. 4A-D**)

To investigate the behaviour of actin networks with or without SPIN90, 20 nM Arp2/3 complex, 50 nM VCA, 0.5 µM profilin, 0 or200 pM mDia1, and various concentrations of SPIN90 were mixed quickly with 0.5 µM 15% Alexa-488 actin in a total volume of 20 µL before being flowed into the chamber. mDia1 elongating filaments were distinguished based on their large length.

To measure the branching rate on preformed actin filaments, 1 µM 15% Alexa-568 labeled actin was incubated at room temperature for at least 30 minutes to generate actin filaments. Before flowing into the chamber, 0.5 µL preformed F-actin was mixed with 19.5 µL of a reaction containing 20 nM Arp2/3 complex, 50 nM VCA, 0.5 µM profilin, 0.5 µM 15% Alexa-488 actin, 0 or 200 pM mDia1, and various concentrations of SPIN90.

Comparing mDia1 affinity for different barbed ends (**Fig. 5A,B,D**)

To compare the affinity of mDia1 for mother filaments versus branches (**Fig. 5A**), 0.5 µM 15% Alexa-568 labelled actin were incubated with 20 nM Arp2/3 and 50 nM VCA for 30 minutes to generate branched actin filaments. After the preformed filaments were flowed in to the flow chamber, the chamber was rinsed with 50 µL buffer. Then, 20 µL of 15% Alexa-488 labelled 0.5 µM G-actin, 0.5 µM profilin, 400 pM mDia1 was flowed into the chamber immediately afterwards. 90 seconds after filaments were exposed to mDia1, the fraction of mother filaments and branches elongating via mDia1 was measured. After a further 90 seconds, the actin filaments were too dense to be analysed.

To compare the fraction of spontaneously nucleated and SPIN90-Arp2/3 nucleated filaments elongating via mDia1 (**Fig. 5B**), 2 µL of spontaneously nucleated actin filaments (1 µM 15% Alexa-568 labelled), and 4 µL of SPIN90-Arp2/3 nucleated actin filaments (0.5 µM 15% Alexa-488 labelled, 25 nM Arp2/3, 250 nM SPIN90) were mixed with 0.5 µM unlabelled actin, 0.5 µM profilin and 200 pM mDia1 in a 20 µL reaction system. Filaments of each subpopulation were identified by the color and intensity of their pointed end regions (Alexa568 labelled for spontaneously nucleated filaments and Alexa488 labelled for SPIN90-Arp2/3 nucleated filaments). After 5 minutes incubation, filaments, with a prenucleated region shorter than 1 µm, were chosen randomly, so that the mDia1 binding fraction of each subpopulation could be measured and compared. Repeat experiments were done inverting

fluorophores to identify each subpopulation, i.e. filaments nucleated spontaneously with 1 µM 15% Alexa-488 labelled G-actin were mixed with filaments nucleated by SPIN90-Arp2/3 and 0.5 µM 15% Alexa-568 labelled G-actin (**Fig. S13A**). No effect of fluorophore labelling of actin was detected.

To compare the fraction of mDia1-bearing barbed ends for filaments nucleated by SPIN90-Arp2/3 in the presence or absence of mDia1 (**Fig 5D**), three 4 µL drops were put on a clean coverslip: a drop of SPIN90-Arp2/3 nucleated actin filaments (0.5 µM 15% Alexa-568 labelled, 25 nM Arp2/3, 250 nM SPIN90), a drop containing profilin, Arp2/3, SPIN90 and mDia1, and a drop of 15% Alexa-488 labelled G-actin. To ensure the rapid and synchronized mixing of the three solutions, 10 µL of buffer was put in the middle of the triangle formed by the three drops on the coverslip, and pipetted up and down. Volumes and concentrations were determined to set up a reaction system containing 0.5 µM 15% Alexa-488 labelled G-actin, 0.6 µM profilin, 25 nM Arp2/3, 250 nM SPIN90, 200 pM mDia1 and filaments prenucleated by SPIN90 Arp2/3. The reaction solution was flowed into an open flow chamber and observed under the microscope. The filaments nucleated in the absence of mDia1 could be distinguished by the color of their pointed end. Five minutes after the components were mixed, the fraction of filaments being elongated by mDia1 in each subpopulation was determined.

To verify that nucleation by mDia1 can be neglected in these experiments, control experiments were done with the same amount of 15% Alexa-488 labelled G-actin, profilin and 200 pM mDia1. After 10 minutes incubation, very few filaments were observed per field of view (**Fig. S13B**), signifying that nucleation by mDia1 can be neglected in our experimental conditions. We also tested the same reaction system, with the full protein mix but without preformed filaments: 0.5 µM 15% Alexa-488 labelled G-actin, 0.6 µM profilin, 25 nM Arp2/3, 250 nM SPIN90, and 200 pM mDia1 were mixed and incubated for 10 minutes. Similar densities of newly formed, mDia1-elongated filaments were observed, indicating that the potential contribution of short preformed filaments which could be misinterpreted as newly nucleated during the experiment was negligible.

Single-molecule imagining

10 nM SPIN90 Cter-647 and 600 nM Arp2/3 were pre-incubated on ice for 10 minutes. 4 µL of the SPIN90 Cter-647 and Arp2/3 mixture were mixed with 1 nM mDia1-549, 0.6 µM profilin and 0.4 µM 15% Alexa-488 labelled G-actin in a 20 µL reaction system. The reaction solution was immediately flowed into an open flow chamber passivated with mPEG silane and PLL-PEG and observed under the microscope. Actin-Alexa488 (1 frame, 100 ms, 488 nm excitation), mDia1-549 (1 frame, 100 ms, 561 nm excitation), SPIN90 Cter-647 (1 frame, 200 ms, 642 nm excitation) were imaged cyclically, every 6s.

Image acquisition for in vitro experiments

The microfluidic devices or the open flow chambers were placed on a Nikon TiE inverted microscope, equipped with a 60x oil-immersion objective. An objective heater (Okolab) maintained the temperature at 25°C on the coverslip. The TIRF setup was controlled by Metamorph, illuminated by 100 mW tunable lasers (iLAS2, Roper Scientific, now Gataca Systems). Images were acquired on an Evolve EMCCD camera (Photometrics). ImageJ software was used to analyze images.

Statistical analysis

Phenotype distribution after gene depletion was compared to cells stably expressing non-silencing shRNA using a Chi-square test (**Table S2**). Cells were imaged on at least two separate days. Values of $p<0.01$ were deemed statistically significant.

The amount of cell death was compared using Welch's two-tailed t-test with unequal standard deviation. Values of $p<0.05$ were deemed statistically significant.

Changes in the proportion of gaps of a given size across conditions was compared with Wilcoxon's rank test. Values of $p<0.01$ were deemed statistically significant.

Changes in cortical thickness, cortical density, and cell area were examined using Welch's t-test. Values of $p<0.05$ were deemed statistically significant.

Changes in actin accumulation rates and cortical stiffness across conditions were examined using a Student t-test. Values of $p<0.01$ were deemed statistically significant.

Supplemental References

1 Chugh, P. *et al.* Actin cortex architecture regulates cell surface tension. *Nat Cell Biol* **19**, 689-697, doi:10.1038/ncb3525 (2017).

2 Bovellan, M. *et al.* Cellular control of cortical actin nucleation. *Curr Biol* **24**, 1628-1635, doi:10.1016/j.cub.2014.05.069 (2014).

3 Cao, L. *et al.* Modulation of formin processivity by profilin and mechanical tension. *Elife* **7**, doi:10.7554/eLife.34176 (2018).

4 Bekker-Jensen, D. B. *et al.* An Optimized Shotgun Strategy for the Rapid Generation of Comprehensive Human Proteomes. *Cell Syst* **4**, 587-599 e584, doi:10.1016/j.cels.2017.05.009 (2017).

5 Funk, J. *et al.* Profilin and formin constitute a pacemaker system for robust actin filament growth. *Elife* **8**, doi:10.7554/eLife.50963 (2019).

6 Cunningham, C. C. *et al.* Actin-binding protein requirement for cortical stability and efficient locomotion. *Science* **255**, 325-327 (1992).

7 Lin, Y. C. *et al.* Genome dynamics of the human embryonic kidney 293 lineage in response to cell biology manipulations. *Nat Commun* **5**, 4767, doi:10.1038/ncomms5767 (2014).

8 Eisenmann, K. M. *et al.* Dia-interacting protein modulates formin-mediated actin assembly at the cell cortex. *Curr Biol* **17**, 579-591, doi:10.1016/j.cub.2007.03.024 (2007).

9 Ren, J. G., Li, Z., Crimmins, D. L. & Sacks, D. B. Self-association of IQGAP1: characterization and functional sequelae. *J Biol Chem* **280**, 34548-34557, doi:10.1074/jbc.M507321200 (2005).

10 Brandt, D. T. *et al.* Dia1 and IQGAP1 interact in cell migration and phagocytic cup formation. *J Cell Biol* **178**, 193-200, doi:10.1083/jcb.200612071 (2007).

11 Seward, M. E., Easley, C. A. t., McLeod, J. J., Myers, A. L. & Tombes, R. M. Flightless-I, a gelsolin family member and transcriptional regulator, preferentially binds directly to activated cytosolic CaMK-II. *FEBS Lett* **582**, 2489-2495, doi:10.1016/j.febslet.2008.06.037 (2008).

12 Ai, H. W., Shaner, N. C., Cheng, Z., Tsien, R. Y. & Campbell, R. E. Exploration of new chromophore structures leads to the identification of improved blue fluorescent proteins. *Biochemistry* **46**, 5904-5910, doi:10.1021/bi700199g (2007).

13 Rappsilber, J., Ryder, U., Lamond, A. I. & Mann, M. Large-scale proteomic analysis of the human spliceosome. *Genome Res* **12**, 1231-1245, doi:10.1101/gr.473902 (2002).

14 Nolen, B. J. *et al.* Characterization of two classes of small molecule inhibitors of Arp2/3 complex. *Nature* **460**, 1031-1034 (2009).

15 Rizvi, S. A. *et al.* Identification and characterization of a small molecule inhibitor of formin-mediated actin assembly. *Chem Biol* **16**, 1158-1168, doi:10.1016/j.chembiol.2009.10.006 (2009).

16 Svitkina, T. M. & Borisy, G. G. Correlative light and electron microscopy of the cytoskeleton of cultured cells. *Methods Enzymol* **298**, 570-592 (1998).

17 Charras, G. T., Hu, C. K., Coughlin, M. & Mitchison, T. J. Reassembly of contractile actin cortex in cell blebs. *J Cell Biol* **175**, 477-490 (2006).

18 Arganda-Carreras, I. *et al.* Trainable Weka Segmentation: a machine learning tool for microscopy pixel classification. *Bioinformatics* **33**, 2424-2426, doi:10.1093/bioinformatics/btx180 (2017).

19 Clark, A. G., Dierkes, K. & Paluch, E. K. Monitoring actin cortex thickness in live cells. *Biophys J* **105**, 570-580, doi:10.1016/j.bpj.2013.05.057 (2013).

20 Biro, M. *et al.* Cell cortex composition and homeostasis resolved by integrating proteomics and quantitative imaging. *Cytoskeleton (Hoboken)* **70**, 741-754, doi:10.1002/cm.21142 (2013).

21 Tinevez, J. Y. *et al.* Role of cortical tension in bleb growth. *Proc Natl Acad Sci U S A* **106**, 18581-18586, doi:10.1073/pnas.0903353106 (2009).

22 Crick, S. L. & Yin, F. C. Assessing micromechanical properties of cells with atomic force microscopy: importance of the contact point. *Biomech Model Mechanobiol* **6**, 199-210, doi:10.1007/s10237-006-0046-x (2007).

23 Sneddon, I. N. The relation between load and penetration in the axisymmetric boussinesq problem for a punch of arbitrary profile. *Int. J. Eng. Sci.* **3**, 10 (1965).

24 Vargas-Pinto, R., Gong, H., Vahabikashi, A. & Johnson, M. The effect of the endothelial cell cortex on atomic force microscopy measurements. *Biophys J* **105**, 300-309, doi:10.1016/j.bpj.2013.05.034 (2013).

25 Barriga, E. H., Maxwell, P. H., Reyes, A. E. & Mayor, R. The hypoxia factor Hif-1alpha controls neural crest chemotaxis and epithelial to mesenchymal transition. *J Cell Biol* **201**, 759-776, doi:10.1083/jcb.201212100 (2013).

26 Barriga, E. H., Franze, K., Charras, G. & Mayor, R. Tissue stiffening coordinates morphogenesis by triggering collective cell migration in vivo. *Nature* **554**, 523-527, doi:10.1038/nature25742 (2018).

27 Nieuwkoop, P. D. The "organization centre". 3. Segregation and pattern formation in morphogenetic fields. *Acta Biotheor* **17**, 178-194 (1967).

28 Kotini, M. *et al.* Gap junction protein Connexin-43 is a direct transcriptional regulator of N-cadherin in vivo. *Nat Commun* **9**, 3846, doi:10.1038/s41467-018-06368-x (2018).

29 Mindell, J. A. & Grigorieff, N. Accurate determination of local defocus and specimen tilt in electron microscopy. *J Struct Biol* **142**, 334-347 (2003).

30 de la Rosa-Trevin, J. M. *et al.* Scipion: A software framework toward integration, reproducibility and validation in 3D electron microscopy. *J Struct Biol* **195**, 93-99, doi:10.1016/j.jsb.2016.04.010 (2016).

31 Scheres, S. H. RELION: implementation of a Bayesian approach to cryo-EM structure determination. *J Struct Biol* **180**, 519-530, doi:10.1016/j.jsb.2012.09.006 (2012).

32 Luan, Q., Liu, S. L., Helgeson, L. A. & Nolen, B. J. Structure of the nucleation-promoting factor SPIN90 bound to the actin filament nucleator Arp2/3 complex. *EMBO J*, doi:10.15252/embj.2018100005 (2018).

33 Otomo, T. *et al.* Structural basis of actin filament nucleation and processive capping by a formin homology 2 domain. *Nature* **433**, 488-494, doi:10.1038/nature03251 (2005).

34 Jurgenson, C. T. & Pollard, T. D. Crystals of the Arp2/3 complex in two new space groups with structural information about actin-related protein 2 and potential WASP binding sites. *Acta Crystallogr F Struct Biol Commun* **71**, 1161-1168, doi:10.1107/S2053230X15013515 (2015).

35 Pettersen, E. F. *et al.* UCSF Chimera--a visualization system for exploratory research and analysis. *J Comput Chem* **25**, 1605-1612, doi:10.1002/jcc.20084 (2004).

36 Balzer, C. J., Wagner, A. R., Helgeson, L. A. & Nolen, B. J. Dip1 Co-opts Features of Branching Nucleation to Create Linear Actin Filaments that Activate WASP-Bound Arp2/3 Complex. *Curr Biol* **28**, 3886-3891 e3884, doi:10.1016/j.cub.2018.10.045 (2018).

37 Breitsprecher, D. *et al.* Rocket launcher mechanism of collaborative actin assembly defined by single-molecule imaging. *Science* **336**, 1164-1168, doi:10.1126/science.1218062 (2012).

38 Le Clainche, C. & Carlier, M. F. Actin-based motility assay. *Curr Protoc Cell Biol* **Chapter 12**, Unit 12 17, doi:10.1002/0471143030.cb1207s24 (2004).

39 Wioland, H. *et al.* ADF/Cofilin Accelerates Actin Dynamics by Severing Filaments and Promoting Their Depolymerization at Both Ends. *Curr Biol* **27**, 1956-1967 e1957, doi:10.1016/j.cub.2017.05.048 (2017).

40 Jegou, A., Carlier, M. F. & Romet-Lemonne, G. Microfluidics pushes forward microscopy analysis of actin dynamics. *Bioarchitecture* **1**, 271-276, doi:10.4161/bioa.1.6.19338 (2011).

41 Zimmermann, D., Morganthaler, A. N., Kovar, D. R. & Suarez, C. In Vitro Biochemical Characterization of Cytokinesis Actin-Binding Proteins. *Methods Mol Biol* **1369**, 151-179, doi:10.1007/978-1-4939-3145-3_12 (2016).